

High variability of particulate organic carbon export along the North Atlantic GEOTRACES section GA01 as deduced from ^{234}Th fluxes

Nolwenn Lemaitre^{1,2,3}, Frédéric Planchon², H  l  ne Planquette², Frank Dehairs³, Debany Fonseca-Batista^{3,4}, Arnout Roukaerts³, Florian Deman³, Yi Tang^{5,6}, Clarisse Mariez², G  rardine Sarthou²

¹Department of Earth Sciences, Institute of Geochemistry and Petrology, ETH-Z  rich, Z  rich, Switzerland

²Laboratoire des Sciences de l'Environnement Marin (LEMAR), UMR 6539, IUEM, Technop  le Brest Iroise, 29280 Plouzan  , France

³Vrije Universiteit Brussel, Analytical, Environmental and Geo-Chemistry, Earth System Sciences research group, Brussels, Belgium

⁴Oceanography Department, Dalhousie University, Halifax, Nova Scotia, Canada

⁵Earth and Environmental Sciences, the Graduate Center, City University of New York, New York, USA

⁶School of Earth and Environmental Sciences, Queens College, City University of New York, Flushing, USA

Correspondence to: Nolwenn Lemaitre (nolwenn.lemaitre@erdw.ethz.ch)

Abstract. In this study we report particulate organic carbon (POC) export fluxes for different biogeochemical basins of the North Atlantic as part of the GEOTRACES GA01 expedition (GEOVIDE, May-June 2014). Surface POC export fluxes were deduced by combining export fluxes of total ^{234}Th with the POC to ^{234}Th ratio of sinking particles at the depth of export. Particles were collected in two size classes ($> 53 \mu\text{m}$ and $1-53 \mu\text{m}$) using *in-situ* pumps and the large size fraction was considered as representative of sinking material. Surface POC export fluxes revealed latitudinal variations between provinces ranging from $1.4 \text{ mmol m}^{-2} \text{ d}^{-1}$ in the Irminger basin where the bloom was close to its maximum, to $12 \text{ mmol m}^{-2} \text{ d}^{-1}$ near the Iberian Margin where the bloom had already declined. In addition to the state of progress of the bloom, variations of the POC export fluxes were also related to the phytoplankton size and community structure. In line with previous studies, the presence of coccolithophorids and diatoms appeared to enhance the POC export flux, while dominance of pico-phytoplankton cells, such as cyanobacteria, resulted in lower fluxes. The POC export to primary production (PP) ratio strongly varied regionally and was generally low ($\leq 14 \%$), except at two stations located near the Iberian margin (35%) and within the Labrador basin (38%), which were characterized by unusual low *in-situ* PP. We thus conclude that the North Atlantic during the GEOVIDE cruise was not as efficient in exporting carbon from the surface, as reported earlier by others. Finally, we also estimated the POC export at 100 m below the surface export depth to investigate the POC transfer efficiencies. This parameter was also highly variable amongst regions, with the highest transfer efficiency at sites where coccolithophorids dominated.

1. Introduction

Through the sinking of particulate biogenic material, the biological carbon pump (BCP) plays a major role on the sequestration of carbon-rich particles in the ocean interior. The North Atlantic harbors one of the most productive spring phytoplankton bloom of the world's ocean (Esaias et al., 1986; Longhurst, 2010), generating an important pulse of biogenic sinking particles (Buesseler et al., 1992; Honjo and Manganini, 1993; Le Moigne et al., 2013a),

39 which accounts up to 18% of the global BCP (Sanders et al., 2014). Yet, a substantial range of carbon export
40 efficiencies (1-47%) has been reported by earlier studies at different locations of the North Atlantic (Buesseler et
41 al., 1992; Buesseler and Boyd, 2009; Ceballos-romero et al., 2016; Herndl and Reinthaler, 2013; Lampitt et al.,
42 2008; Moran et al., 2003; Mouw et al., 2016; Thomalla et al., 2008), directly questioning about how carbon export
43 efficiency varies at a trans-Atlantic scale and what are the controlling factors.

44 The international GEOTRACES program aims to measure trace elements and isotopes along full-depth ocean
45 sections through each of the major ocean basins in order to provide maximum scientific rewards on a global scale
46 (GEOTRACES, 2006). The GEOVIDE GA01 section in the high-latitude North Atlantic (15 May - 30 June 2014;
47 R/V Pourquoi Pas?), was a French contribution to this global survey. The studied area crossed five basins
48 differentiated by their distinct biogeochemical and hydrodynamic characteristics: the Iberian basin, the west
49 European basin, the Icelandic basin, the Irminger basin and the Labrador basin (Fig.1).

50 The low nutrient availabilities (surface nitrate and silicate concentrations $< 1 \mu\text{mol L}^{-1}$; nutrient analyses according
51 to Aminot and K  rouel, 2007) in the Iberian basin limits the biomass development giving the opportunity to pico-
52 phytoplankton, such as cyanobacteria, to grow (~ 35% of the total Chl-*a* at Station 13; Tonnard et al., in prep.;
53 pigment analyses according to Ras et al., 2008), a situation which is typical for the North Atlantic subtropical gyre
54 (Moore et al., 2008; Zehr and Ward, 2002). The Iberian basin can also be influenced by a local upwelling, close
55 to the Iberian margin (Costa Goela et al., 2016; Z  niga et al., 2016; <http://marine.copernicus.eu/>) and potentially
56 fueling the area with nutrient-rich, but upwelling was not active during GEOVIDE (Shelley et al., 2016).

57 In the subpolar region, in the Irminger and Labrador basins, phytoplankton growth is strongly light-limited
58 seasonally (Riley, 1957) and the key parameter for alleviating these limitations is the progressive shoaling of the
59 mixed layer. There, micro-phytoplankton, such as diatoms, dominate the phytoplankton bloom ($\geq 50\%$ of the total
60 Chl-*a*; Tonnard et al., in prep.). Both basins were influenced by strong hydrodynamic features, such as the Irminger
61 gyre, the Eastern Greenland Current (EGC), the Western Greenland Current (WGC), the Labrador Current (LC;
62 Zunino et al., 2017) and the subduction of the Labrador Seawater (LSW) which was particularly intense (1700 m-
63 deep convection) during the winter 2013-2014 (Kieke and Yashayaev, 2015).

64 Between the subtropical and subpolar regions, the west European and Icelandic basins represent a transition zone
65 where nutrients and/or light can limit primary production (Henson et al., 2009). During GEOVIDE, the silicic acid
66 stock was low ($\leq 1 \mu\text{mol L}^{-1}$) leading to the growth of nano-phytoplankton, such as haptophytes including
67 coccolithophorids (between 45 and 80% of the total Chl-*a*; Tonnard et al., in prep.). This region is influenced by
68 the Eastern Reykjanes Ridge Current (ERRC) and by the North Atlantic Current (NAC) with the southernmost
69 sub-branch evolving in a cyclonic eddy and the sub-arctic front (SAF). SAF separates cold and fresh waters from
70 the subpolar region and the warm and salty waters from the subtropical region (Zunino et al., 2017).

71 The North Atlantic is thus a heterogeneous basin in terms of nutrient status, phytoplankton communities and
72 hydrodynamic features.

73 This is of a crucial importance as ecosystem structure is thought to play an important role on the BCP. Guidi et al.
74 (2009) suggested that phytoplankton composition explained 68% of the variance in POC flux at 400 m. High
75 export efficiencies are reported in productive regions where diatoms dominate, but the exported material is
76 relatively labile and prone to remineralisation leading to low transfer efficiency and low deep export flux (Guidi
77 et al., 2009). Conversely, in oligotrophic regions, where diatoms are largely absent, primary production is low and
78 mostly regenerated. Consequently, export efficiencies are low but the eventual exported material is likely less

79 prone to dissolution - remineralisation, resulting in high transfer efficiencies (Henson et al., 2012; Lam et al., 2011;
80 Lima et al., 2014; Marsay et al., 2015). Phytoplankton size structure has also been shown to be an important factor
81 in controlling the POC export fluxes. Guidi et al. (2015) highlighted that the exported POC was more refractory
82 and the remineralisation depth was deeper when the fraction of micro-phytoplankton decreased or the fraction of
83 pico-phytoplankton increased.

84 Due to the complex impact of these biogeochemical factors on the POC export and according to the distinct
85 features of each biogeochemical basin, the efficiency of the North Atlantic to transfer POC to the deep ocean
86 deserves more study.

87 In this context, we investigated POC export fluxes derived from the Thorium-234 (^{234}Th) approach along a transect
88 in the high-latitude North Atlantic, from the Iberian margin to the sub-arctic Irminger and Labrador Seas. ^{234}Th , a
89 highly particle reactive element with a short half-life (24.1 d), is widely used to explore particle export over short
90 time events such as phytoplankton blooms (Bhat et al., 1969; Buesseler et al., 1992; Coale and Bruland, 1985;
91 Cochran and Masqué, 2003). A deficit of ^{234}Th with respect to its radioactive parent ^{238}U (conservative in seawater)
92 is usually observed in the upper water column where particles sink. In the subsurface waters any excess of ^{234}Th
93 relative to ^{238}U , is taken to reflect particle break-up and remineralisation by heterotrophic bacteria and/or
94 zooplankton (Buesseler et al., 2008; Maiti et al., 2010; Savoye et al., 2004). A ^{234}Th flux can be converted into a
95 POC flux by using the POC: ^{234}Th ratio of sinking particles at the depth of export (Buesseler et al., 2006).

96 In this study, we discuss carbon export fluxes determined at the base of the deficit zone according to the
97 biogeochemical properties found in each basins, with special emphasis on the stage and intensity of the bloom as
98 well as on the phytoplankton community structure. Using estimates of primary production from shipboard
99 incubations and satellite-derived Chl-*a*, we explore surface export efficiencies at different time scales over the
100 studied area. In addition and using deep carbon export, we investigate POC transfer efficiency in the upper
101 mesopelagic.

102 2. Methods

103 2.1. Total ^{234}Th and ^{238}U

104 Total ^{234}Th activities were determined from 4 L unfiltered seawater samples collected with 12L Niskin bottles.
105 Usually, 17 or 18 depths were sampled between the surface and 1000-1500 m, except at Stations 26 and 77 where
106 only 9 and 15 depths were sampled, respectively (Table S1). Deep samples (between 1000 and 3500 m) were taken
107 for the calibration of the low level beta counting (Rutgers van der Loeff et al., 2006) based on the knowledge that
108 ^{234}Th and ^{238}U are generally in secular equilibrium at such depths (in this study, the deep ocean average $^{234}\text{Th}/^{238}\text{U}$
109 ratio = 1.00 ± 0.02 ; $n=15$). Seawater samples were processed following the method developed by Pike et al. (2005).
110 Samples were acidified at pH 2 and spiked with a ^{230}Th yield monitor in order to estimate the ^{234}Th recovery during
111 the sample processing. After 12 hours of equilibration, pH was increased to 8.5 and KMnO_4 and MnCl_2 (analytical
112 grade, Merck) were added to form a manganese oxide precipitate. After a further 12 hours of equilibration, samples
113 were filtered on quartz-microfiber discs (QMA, Sartorius, 1 μm nominal porosity, 25 mm diameter). On board,
114 filters were dried overnight, mounted on nylon holders, and covered with Mylar and aluminum foil. The activity
115 of ^{234}Th on each sample was counted using low level beta counters (RISØ, Denmark). Beta activity counting was
116 continued until a relative standard deviation (RSD) $\leq 2\%$ was reached. At the home-laboratory, residual beta

117 activity was measured for each sample after a delay of six ^{234}Th half-lives (~ 6 months) and these residual counts
118 were subtracted from the gross counts obtained on-board. All samples were then processed for Th recovery using
119 ^{229}Th as a second yield tracer. To do so, filters were dismounted from the nylon holders and transferred to clean
120 30 mL teflon vials (Savillex). All samples were spiked with ^{229}Th , dissolved in a mix of 8M HNO_3 /1M H_2O_2
121 (suprapur grade, Merck), heated overnight and filtered through Acrodisc® syringe filters (Pall, Nylon membrane,
122 nominal porosity=0.2 μm , diameter=25 mm). Part of the filtrate was pre-concentrated by evaporation and the
123 residue diluted in 1.4 M HNO_3 (suprapur grade, Merck). ^{230}Th and ^{229}Th concentrations were measured by sector
124 field inductively coupled plasma mass spectrometry (SF-ICP-MS, Element 2, Thermo Scientific) in low resolution
125 mode. Each sample was analyzed 3 times and the precision of the ^{230}Th : ^{229}Th ratios averaged 1.2% (RSD), which
126 is within the range indicated by Pike et al. (2005). The total ^{234}Th recovery, involving all the steps described above,
127 was $91 \pm 14\%$ (n=200). Uncertainty of total ^{234}Th activity, estimated from error propagation, was between 0.04
128 and 0.10 dpm L^{-1} .

129 The ^{238}U activity was deduced from salinity using the Eq. 1, given by Owens et al. (2011):

$$130 \quad {}^{238}\text{U} = 0.0786 \times S - 0.315 \quad (1)$$

131 where ^{238}U is the ^{238}U activity in dpm L^{-1} and S is salinity.

132 **2.2. Particulate ^{234}Th and POC sampling and analysis**

133 Suspended particles were collected using *in-situ* large-volume filtration (100-1600 L) systems (Challenger
134 Oceanics and McLane pumps; ISP hereafter for “*in-situ* pumps”) through paired 142 mm-diameter filters: a 53 μm
135 mesh nylon screen (SEFAR-PETEX®; polyester) and a 1 μm pore size quartz-microfiber filter (QMA, Sartorius),
136 respectively. The small size fraction (1-53 μm) is referred to hereafter as SSF and the large size fraction (> 53 μm)
137 as LSF. Prior to the cruise, filters were cleaned as follows: PETEX screens were soaked in 0.6 M HCl (Normapur,
138 Merck), rinsed with Milli-Q water, dried at ambient temperature in a laminar flow hood, and stored in clean plastic
139 bags; QMA filters were pre-combusted at 450 °C for 4 h and stored in aluminum foils until use. ISP were deployed
140 between 15 and 800 m on a stainless steel cable and the pumping time was approximatively 2-3 h (Table S2).

141 After collection, filters were processed on board. The 142 mm PETEX screen was cut into quarters using a clean
142 scalpel and two quarters were processed in this study. Particles were rinsed-off from the PETEX screen using 0.45
143 μm filtered seawater under a laminar flow hood. For one quarter of the PETEX screen, the rinsed-off particles
144 were re-filtered on a silver filter (SterliTech, porosity=0.45 μm , diameter=25 mm) and for the other quarter on a
145 GF/F filter (Whatman®, porosity=0.7 μm , diameter=25 mm). The QMA filters were sub-sampled with a perspex
146 punch of 25 mm diameter. Silver, GF/F and QMA filters were dried overnight and prepared for beta counting (see
147 section 2.1). After counting the residual beta activity (~ 6 months later), samples were prepared for POC,
148 particulate nitrogen (PN) analyses along with their $\delta^{13}\text{C}$ and $\delta^{15}\text{N}$ isotopic compositions (here we present only POC
149 data). Filters were dismounted from filter holders and fumed with HCl vapor overnight inside a glass desiccator to
150 remove the carbonate phase. Samples were dried, packed in precombusted (450 °C overnight) silver cups, and
151 analyzed with an elemental analyzer – isotope ratio mass spectrometer (EA-IRMS, Delta V Plus, Thermo
152 Scientific). Acetanilide standards were used for the calibration. The detection limits and C blanks were respectively
153 0.63 and 0.80 μmol for Ag filters (n=11) and were 0.49 and 1.52 μmol for QMA filters (n=13).

154 The POC concentrations and ^{234}Th activities compared well between silver and GF/F filter types pointing to the
 155 rather homogenous distribution of the particles on the Petex screen ($^{234}\text{Th}_{\text{GFF}} = 0.63 \times ^{234}\text{Th}_{\text{silver}} + 0.01$ with $r^2=0.88$,
 156 $p\text{-value}<0.01$ and $n=58$; and $\text{POC}_{\text{GFF}} = 0.86 \text{ POC}_{\text{silver}} + 0.08$ with $r^2=0.90$, $p\text{-value}<0.01$ and $n=58$; Fig. S1),
 157 although concentrations from GF/F filters were systematically lower than those from silver filters, most likely
 158 because of the different pore size filter ($0.7 \mu\text{m}$ for GF/F filter vs $0.45 \mu\text{m}$ for silver filter).

159 2.3. Export fluxes of ^{234}Th

160 Thorium-234 activity in surface waters can be described using a simple mass balance equation (Savoye et al.,
 161 2006), which accounts for production from ^{238}U decay, ^{234}Th decay, sinking flux and transport as follow:

$$162 \quad \frac{dA_{\text{Th}}}{dt} = \lambda A_{\text{U}} - \lambda A_{\text{Th}} - P + V \quad (2)$$

163 where A_{Th} is the activity of total ^{234}Th in dpm L^{-1} ; A_{U} is the salinity-derived activity of ^{238}U in dpm L^{-1} , λ is the
 164 ^{234}Th decay constant (0.0288 d^{-1}); P is the net removal of ^{234}Th on sinking particles in $\text{dpm L}^{-1} \text{ d}^{-1}$; V is the sum of
 165 the advective and diffusive fluxes in $\text{dpm L}^{-1} \text{ d}^{-1}$.

166 Assuming steady state (constant total ^{234}Th activity with time) and neglecting the physical term V (Buesseler et
 167 al., 1992), the net export flux of particulate ^{234}Th can be determined using the following equation:


$$168 \quad P = \lambda \int_0^z (A_{\text{U}} - A_{\text{Th}}) dz \quad (3)$$

169 where P is the integrated flux of ^{234}Th from the surface to the depth z in $\text{dpm m}^{-2} \text{ d}^{-1}$. Eq. 3 has been solved for z
 170 taken as the depth (Eq) at the base of the ^{234}Th deficit zone (Eq = depth where ^{234}Th activity is back to secular
 171 equilibrium with ^{238}U) as well as for z representing the base of the primary production zone (PPZ), i.e. the depth
 172 where *in-situ* fluorescence was only 10% of its maximum value (Owens et al., 2014). The Eq depth matched
 173 relatively well with the PPZ depth, and on average, difference between both was only 16 m, with the largest
 174 difference ($\sim 60 \text{ m}$) at Stations 1, 32 and 51 (Fig. 2). Considering that there can be export (or remineralisation)
 175 below or above the PPZ depth, only the export fluxes at the Eq depth will be discussed as they represent the fully-
 176 integrated depletion of ^{234}Th in the upper waters and thus the maximal export. The validity of the assumptions
 177 used for solving Eq. 3 is discussed in Section 4.1.

178 In Section 4.1.2, we attempt to calculate the ^{234}Th fluxes at the Eq depth by using a non-steady state (NSS) model
 179 (Savoye et al., 2006), which can be described as follows:

$$180 \quad P = \lambda \left[\frac{A_{\text{U}} (1 - e^{-\lambda \Delta t}) + A_{\text{Th1}} e^{-\lambda \Delta t} - A_{\text{Th2}}}{1 - e^{-\lambda \Delta t}} \right] \quad (4)$$


181 where Δt is the time interval between two visits of a single station; A_{Th1} and A_{Th2} are the ^{234}Th activities at the first
 182 and second visits, respectively. Without time series data, the calculation should not be performed *sensu stricto*
 183 (Buesseler et al., 1992; Savoye et al., 2006) but we chose to set the initial conditions for each station, as done by
 184 Rutgers van der Loeff et al. (2011) in the South Atlantic. Satellite-derived PP data were used to estimate the starting
 185 date of the bloom (i.e., when there is a PP increase of 30% above the winter value) and ^{234}Th was assumed to be
 186 in equilibrium with ^{238}U at this time point. The time interval (Δt) for the calculations stretched from the bloom
 187 start until the sampling date. All physical terms were considered negligible.

188 To estimate the intensity of shallow remineralization, export flux was also calculated for the Eq+100 m depth
 189 horizon. In case of any ^{234}Th excess below  due to remineralisation, export fluxes integrated until Eq+100 m
 190 will be less than when integrated until Eq. Following Black et al. (2017) the reduction of the ^{234}Th flux, R100, is
 191 expressed as:

$$192 \quad R100 = P_{\text{Eq}} - P_{\text{Eq}+100} \quad (5)$$

193 where R100 is the flux reduction in $\text{dpm m}^{-2} \text{d}^{-1}$ and P is the ^{234}Th export flux estimated at Eq or Eq+100.

194 **2.4. Scavenging fluxes of ^{234}Th**

195 To estimate the rate of removal of  ^{234}Th from the dissolved to the particulate form, i.e., the scavenging flux of
 196 ^{234}Th (Coale and Bruland, 1985), we deduced the dissolved ^{234}Th activities by subtracting the particulate
 197 (SSF+LSF) from the total ^{234}Th activities, keeping in mind, though, that the sampling method for the total and
 198 particulate phases differed. Because the sampling resolution was different, total ^{234}Th data were averaged at the
 199 sampling depth of particulate ^{234}Th .

200 The mass balance equation for dissolved ^{234}Th can be written as follows:

$$201 \quad \frac{dA_{\text{Thd}}}{dt} = \lambda A_{\text{U}} - \lambda A_{\text{Thd}} - J + V \quad (6)$$

202 where A_{Thd} is the activity of dissolved ^{234}Th in dpm L^{-1} ; A_{U} and λ are defined in Eq. 2; J is the net removal flux
 203 from the dissolved to the particulate form (scavenging flux) in $\text{dpm L}^{-1} \text{d}^{-1}$; and V is the sum of the advective and
 204 diffusive fluxes in $\text{dpm L}^{-1} \text{d}^{-1}$.

205 Using again the steady state assumption (dissolved ^{234}Th activities remain constant over time) and ignoring the
 206 physical terms (V), Eq. 6 becomes:

$$207 \quad J = \lambda \int_0^z (A_{\text{U}} - A_{\text{Thd}}) dz \quad (7)$$

208 where J in $\text{dpm m}^{-2} \text{d}^{-1}$ is the net flux of scavenging integrated to the depth z. In our case, the calculation was
 209 performed at the Eq depth for comparison with the ^{234}Th export flux (P in Eq. 3).

210 The comparison between the export flux (P) and scavenging flux (J) in terms of P/J ratio (export ratio) offers a
 211 valuable metric for estimating the export efficiency of ^{234}Th . A low P/J ratio (< 0.5) indicates that the removal of
 212 dissolved ^{234}Th is controlled by sorption onto suspended particles rather than export. Conversely, a high P/J ratio
 213 (> 0.5) indicates that ^{234}Th is preferentially exported rather than adsorbed and is thus efficiently removed from the
 214 upper waters.


215 **2.5. POC: ^{234}Th ratios and POC export fluxes**

216 We estimated POC export fluxes by multiplying the ^{234}Th export flux with the POC: ^{234}Th ratio, both determined
 217 at the Eq depth. A power law fit was used to determine the POC: ^{234}Th ratios at Eq (Fig. 3). Errors of the POC: ^{234}Th
 218 ratios extrapolated at the Eq depth are deduced from the power law fit, using a root sum of square method. This
 219 error is much larger than analytical errors of both POC concentrations and particulate ^{234}Th activities. POC fluxes

220 were determined by using the POC:²³⁴Th ratios of the LSF (> 53 μm) as well as the SSF (1-53 μm) samples, and
221 both estimations were compared (Table 2).

222 The POC fluxes were between 1.1 to 1.5 fold higher when using the SSF POC:²³⁴Th ratio, except at stations 1, 26
223 and 64. However, when considering the uncertainties, POC fluxes based on SSF and LSF POC:²³⁴Th ratios were
224 not significantly different, and as we did not have the possibility to compare the POC:²³⁴Th ratios with those from
225 sediment traps, we cannot affirm that the small particles participated to the export. As large and rapidly sinking
226 particles usually drive most of the export (Lampitt et al., 2001; Villa-Alfageme et al., 2016), most of the studies
227 dedicated to POC export fluxes in the North Atlantic used the POC:²³⁴Th ratios from the LSF (see Le Moigne et
228 al., 2013b; Puigcorbé et al., 2017). Therefore, only the POC fluxes determined with the POC:²³⁴Th ratios from the
229 LSF will be discussed (Table 3).

230 **2.6. In-situ primary production**

231 In order to determine the *in-situ* daily PP, stable isotope incubations were conducted using seawater collected at
232 different euphotic zone depths selected using photosynthetically active radiation (PAR) profiles, as described in
233 more detail in Fonseca-Batista et al. (2018). At each station, seawater was sampled from 3 to 6 depths (from 54 to
234 0.2% of surface PAR) and incubated on deck with a H¹³CO₃⁻ enriched substrate. After 24 h, incubated samples
235 were filtered through microglass fiber filters (MGF, 0.7 μm porosity, Sartorius). At the home-laboratory, POC
236 concentrations and isotopic composition were analyzed by EA-IRMS and uptake rates were deduced following the
237 Hama et al. (1983) method. Daily PP was then estimated by integrating the uptake rates from the surface down to
238 0.2% of surface PAR, which was located between 48 and 116 m depending on the station. The 0.2% of surface
239 PAR depth was roughly corresponding to the Eq depth although, at few stations  2 m difference was observed.
240 Note that at Station 51, PP was determined 24 h after the sampling of the total ²³⁴Th, particulate ²³⁴Th and POC.

241 **2.7. Satellite primary production**

242 PP was also obtained from satellite data products with a 9 km spatial resolution and 8-day temporal resolution,
243 available from the Ocean Productivity website at Oregon State University
244 (http://www.science.oregonstate.edu/ocean_productivity/) and obtained from MODIS and SeaWiFS satellites.
245 Three different models can be used to obtain satellite-derived PP: the standard Vertically Generalized Production
246 Model (VGPM; (Behrenfeld and Falkowski, 1997), the Eppley-VGPM (Eppley, 1972) and the Carbon-Based
247 Production Model (CbPM; Behrenfeld et al., 2005; Westberry et al., 2008). Among the model outputs, VGPM
248 derived PP (VGPM-PP) are closest to the *in-situ* PP measurements during our study (Fig. 4). Therefore, VGPM-
249 PP is used in later discussion.

250 VGPM-PP data were averaged over 5 × 5 pixel boxes corresponding to a surface area of 2025 km² (45 km×45 km)
251 centered on the different sampling stations and the VGPM-PP was averaged for the week (8 days), the month (32
252 days) and the whole productive period prior to the sampling date. The whole productive period is the period
253 between the bloom start (defined by a PP increase of 30% above the winter value) and the sampling date (Fig. 5).
254 Differences between the different VGPM-PP estimates were smaller than a factor of 1.5.

255 3. Results

256 3.1. The Iberian basin (Stations 1 and 13)

257 Stations 1 and 13 were sampled 10 to 12 weeks after the start of the bloom (Fig. 4). At these stations, PP increased
258 very early in the year (early to mid-March) and collapsed rapidly (end of March to mid-April). Within the Iberian
259 basin, low *in-situ* PP were determined (Table 3), with one of the lowest values measured at Station 1 ($33 \text{ mmol m}^{-2} \text{ d}^{-1}$) and a moderate PP at Station 13 ($79 \text{ mmol m}^{-2} \text{ d}^{-1}$; Fonseca-Batista et al., 2018; this issue).

261 In line with low *in-situ* PP, low POC concentrations and particulate ^{234}Th activities were determined in the Iberian
262 basin (Table S2). POC: ^{234}Th ratios were low in both size fractions at Station 13, while Station 1 had high ratios,
263 reaching $31 \mu\text{mol dpm}^{-1}$ in surface for the LSF (Fig. 3). Similarly, Station 13 had the lowest LSF POC: ^{234}Th ratio
264 extrapolated at Eq whereas Station 1 had one of the highest ratios (Table 3).

265 The $^{234}\text{Th}/^{238}\text{U}$ ratios were in the median of the range observed along the transect and reached minima of 0.68 and
266 0.70 in the upper 40 m at Stations 1 and 13, respectively (Fig. 2). Interestingly, these two stations vary also in their
267 total particulate ^{234}Th (sum of the SSF and LSF) over total ^{234}Th ratios with only 9% of the ^{234}Th in the particulate
268 phase at Station 1 and 28% at Station 13 (in the median of those observed elsewhere along the transect). At both
269 stations, the ^{234}Th export fluxes at the Eq depth were slightly higher than the median value observed along the
270 transect ($1135 \text{ dpm m}^{-2} \text{ d}^{-1}$, $n=11$), reaching 1264 and $1418 \text{ dpm m}^{-2} \text{ d}^{-1}$ at Stations 1 and 13, respectively (Table
271 1). Compared to Station 1, the ^{234}Th scavenging flux was ~ 2 fold higher at Station 13 (1509 and $2898 \text{ dpm m}^{-2} \text{ d}^{-1}$,
272 respectively; Table 1). Consequently, the export ratio (P/J) was higher at Station 1, reaching 0.84, compared to
273 Station 13 (P/J ratio=0.49; Fig. 6). This indicates a balanced situation between P and J fluxes at Station 13 and a
274 more efficient export of ^{234}Th by sinking particles at Station 1.

275 Below Eq, significant excesses of ^{234}Th relative to ^{238}U (i.e., $^{234}\text{Th}/^{238}\text{U}$ ratio > 1.1) were observed at both stations,
276 indicating particle degradation (Fig. 2). However, significant shallow remineralisation was only observed at
277 Station 13 for which the R100 value was above uncertainty, reaching $410 \pm 218 \text{ dpm m}^{-2} \text{ d}^{-1}$ (Table 1). This
278 represents a flux reduction of 30% relative to the surface export flux.

279 Similarly, POC export fluxes varied between both stations with the highest (albeit the high associated error; 12
280 $\text{mmol m}^{-2} \text{ d}^{-1}$ at Station 1) and one of the lowest ($2.2 \text{ mmol m}^{-2} \text{ d}^{-1}$ at Station 13) fluxes along the transect observed
281 within this basin.

282 3.2. The west European basin (Stations 21 and 26)

283 Along the year 2014, the west European basin was the most productive with the highest PP peak observed at
284 Station 21 ($403 \text{ mmol m}^{-2} \text{ d}^{-1}$), 13 days before the sampling. At Station 26, the sampling took place during a
285 secondary PP increase (Fig. 4 and 5). At sampling time, during the bloom development, the basin was very
286 productive with *in-situ* PP reaching 135 and $174 \text{ mmol m}^{-2} \text{ d}^{-1}$ at Stations 21 and 26, respectively (Table 3).

287 Along with the high POC concentrations and particulate ^{234}Th activities were measured
288 averaging $3.7 \mu\text{mol L}^{-1}$ and 0.2 dpm L^{-1} for the LSF and, $5.4 \mu\text{mol L}^{-1}$ and 0.5 dpm L^{-1} for the SSF (Table S2). For
289 both size fractions, POC: ^{234}Th ratios were high in the upper water column, reaching a maximum of $30 \mu\text{mol dpm}^{-1}$
290 for the LSF in surface waters at Station 21 (Fig. 3). At the Eq depth, the POC: ^{234}Th ratios for the LSF were in
291 the median of those determined along the transect ($4.4 \mu\text{mol dpm}^{-1}$, $n=11$) with nevertheless a lower ratio at Station
292 21 ($2.6 \mu\text{mol dpm}^{-1}$; Table 3).

293 The lowest $^{234}\text{Th}/^{238}\text{U}$ ratios were observed in the surface waters of the west European basin reaching minima of
294 0.57 and 0.77 at Stations 21 and 26, respectively (Fig. 2). Moreover, these low ratios were observed deeper in the
295 water column compared to the other basins. The integration of the ^{234}Th deficit from the surface to the Eq depth
296 led thus to high ^{234}Th export fluxes at both stations. The ^{234}Th export flux at Station 21 was one of the highest
297 observed along the transect, reaching $1873 \text{ dpm m}^{-2} \text{ d}^{-1}$ (Table 1). The ^{234}Th scavenging fluxes were also among
298 the highest observed along the transect, reaching 3917 and $2839 \text{ dpm m}^{-2} \text{ d}^{-1}$ at Stations 21 and 26, respectively
299 (Table 1). The resulting export ratio (P/J) was about 0.5 at both stations, indicating a balanced situation between
300 export and scavenging fluxes.

301 Excess of ^{234}Th relative to ^{238}U below Eq, was observed at both stations, with $^{234}\text{Th}/^{238}\text{U}$ ratios reaching 1.14 at
302 300 m for Station 21 (Fig. 2; Table S1). Consequently, the R100 value at this station was significant 10 ± 255
303 $\text{dpm m}^{-2} \text{ d}^{-1}$; Table 1), representing a 20% ^{234}Th flux reduction.

304 Relatively high POC export fluxes at Eq were observed in the west European basin, reaching respectively 4.8 and
305 7.9 $\text{mmol m}^{-2} \text{ d}^{-1}$ at Stations 21 and 26. For the same area, other studies reported similar POC export fluxes during
306 May (Thomalla et al., 2008), and July-August (Lampitt et al., 2008; Le Moigne et al., 2013). However, Buesseler
307 et al. (1992) report much higher POC fluxes (up to $41 \text{ mmol m}^{-2} \text{ d}^{-1}$) for April-May during the North Atlantic
308 Bloom Experiment, highlighting an important temporal variability of POC export flux in this basin (Fig. 7).

309 3.3. The Icelandic basin (Stations 32 and 38)

310 In general, the different fluxes in the Icelandic basin were similar to those in the west European basin.
311 The bloom period started in May, one month before the sampling and the bloom maximum occurred after the
312 cruise (Fig. 4). Nevertheless, the basin was highly productive at Station 32 with *in-situ* PP reaching 105 mmol m^{-2}
313 d^{-1} and was relatively productive at Station 38 ($68 \text{ mmol m}^{-2} \text{ d}^{-1}$; Table 3 and Fig. 4 and 5).

314 POC concentrations and particulate ^{234}Th activities were relatively high, but unlike the west European basin the
315 highest concentrations and activities were found in the SSF, reaching $5.8 \mu\text{mol L}^{-1}$ and 0.4 dpm L^{-1} , respectively
316 at Station 32 (Table S2). For surface waters of both stations, POC: ^{234}Th ratios in the SSF exceeded those in the
317 LSF (Fig. 3) but ratios were similar between both fractions at Eq depth (difference less than a factor of 1.1).
318 The ratios extrapolated to Eq for the LSF were 3.6 and $4.2 \mu\text{mol dpm}^{-1}$ at Stations 32 and 38, respectively and
319 were in the median of the range along the transect (Table 3).

320 As for the west European basin, $^{234}\text{Th}/^{238}\text{U}$ ratios were low with station 38 having the lowest value for the whole
321 transect (0.50 in the surface; Fig. 2). Low ratios were also observed deeper in the water column and the combination
322 yielded the highest ^{234}Th export fluxes at Eq, reaching $2282 \pm 119 \text{ dpm m}^{-2} \text{ d}^{-1}$ at Station 32 (Table 1). While the
323 ^{234}Th scavenging flux was high at Station 32, reaching $3690 \text{ dpm m}^{-2} \text{ d}^{-1}$, it was much lower at Station 38 (1495
324 $\text{dpm m}^{-2} \text{ d}^{-1}$; Table 1). The export ratios (P/J) slightly exceeded the median value along the transect, reaching 0.62
325 and 0.76 at Stations 32 and 38, respectively. Despite similarities with the west European basin, the Icelandic basin
326 appeared more efficient to export ^{234}Th by sinking particles.

327 Below the Eq depth, there was no significant excess of ^{234}Th relative to ^{238}U , resulting in R100 values being close
328 or below uncertainty and indicating absence of significant shallow remineralisation.


329 One of the highest POC export fluxes along the transect was determined at Station 32, reaching $8.3 \text{ mmol m}^{-2} \text{ d}^{-1}$
330 while the POC flux at Station 38 was lower ($4.8 \text{ mmol m}^{-2} \text{ d}^{-1}$). Such POC export fluxes are lower than those

331 reported in earlier studies, ranging from 0.8 to up to 52 mmol m⁻² d⁻¹; Ceballos-romero et al., 2016; Giering et al.,
332 2016; Martin et al., 2011; Sanders et al., 2010; Fig. 7).


333 3.4. The Irminger basin (Stations 44 and 51)

334 The ship crossed the Irminger basin one month after the beginning of the bloom and sampling occurred just 1 week
335 (Station 44) to 3 weeks (Station 51) after the peak of the bloom (Fig. 4). At sampling time, the *in-situ* PP was
336 amongst the highest observed along the whole section, reaching respectively 137 and 166 mmol m⁻² d⁻¹ at Stations
337 44 and 51. Such high values, in line with the satellite data, suggest that the bloom was still ongoing when visiting
338 these two stations (Table 3 and Fig. 4 and 5).

339 POC concentrations and particulate ²³⁴Th activities were overall highest at these two stations, reaching 17 μmol L⁻¹
340 and 1.2 dpm L⁻¹ for the SSF and 4.0 μmol L⁻¹ and 0.5 dpm L⁻¹ for the LSF at Station 44, respectively (Table S2).
341 POC:²³⁴Th ratios were moderate for both size fractions, reaching 14 μmol dpm⁻¹ for the SSF at Station 44 and 12
342 μmol dpm⁻¹ at Station 51 in the surface waters (Fig. 3). At the Eq depth, the extrapolated POC:²³⁴Th ratios were
343 similar between both size fractions at Station 51 but were 1.7 fold higher in the SSF at Station 44. The POC:²³⁴Th
344 ratio at Eq in the LSF at Station 44 fitted the median of the ranges determined along the transect, while the ratio at
345 Station 51 was relatively lower (2.9 μmol dpm⁻¹, Table 3).

346 The ²³⁴Th/²³⁸U ratios in the surface waters were higher than at other stations, reaching minima of 0.79 and 0.78 at
347 Stations 44 and 51, respectively. These low ²³⁴Th deficits were also restricted to the upper layer, especially at
348 Station 44 where the Eq depth was 40 m (Fig. 2). The particulate ²³⁴Th (sum of the SSF and LSF) contribution to
349 total ²³⁴Th ratios varied widely, from 27% at Station 51 (in the median of those observed elsewhere along the
350 transect) to 94% at Station 44. The extremely high fraction of particulate ²³⁴Th at Station 44 reflects an important
351 particle concentration in surface waters.  high particulate fraction in the upper layer did not induce a high
352 export fluxes, since Station 44 had the lowest ²³⁴Th export flux (321 ± 66 dpm m⁻² d⁻¹; Table 1) of all stations. As
353 a result, scavenging fluxes were much higher in this basin, reaching respectively 1802 and 2189 dpm m⁻² d⁻¹ at
354 Stations 44 and 51. This leads to very low P/J ratios in the Irminger basin (as low as 0.2 at Station 44), suggesting
355 that export of ²³⁴Th is particularly inefficient in this basin, in agreement with the low export flux and the high
356 particulate fraction in the upper layer.

357 Below the Eq depth, there was no significant excess of ²³⁴Th relative to ²³⁸U, reflecting no evidence for significant
358 shallow remineralisation, with R100 values being either negative or below uncertainty.

359 The Irminger basin was characterized by low POC export fluxes (1.4 and 2.7 mmol m⁻² d⁻¹ at Stations 44 and 51,
360 respectively). In the literature, a relatively large range of POC export fluxes has been reported for this basin.
361 Puigcorbé et al. (2017) observed POC export fluxes ranging from 1.5 to 43 mmol m⁻² d⁻¹. Ceballos-Romero et al.
362 (2016) also determined much higher POC fluxes compared to those observed in the present study, with differences
363 reaching factors of 27 and 19  month before and after our sampling, respectively (Fig. 7).

364 3.5. The Labrador basin (Stations 64, 69 and 77)

365 Stations of the Labrador basin were sampled approximatively one month after the beginning of the bloom. Station
366 64 was sampled just after a second peak of the bloom while Stations 69 and 77 were sampled one week after this
367 peak (Fig. 4). At sampling time, the *in-situ* PP was low in the Labrador basin, ranging from 27 to 80 mmol m⁻² d⁻¹

368 ¹ at Stations 69 and 77, respectively (Table 3). In agreement with the satellite data shown in Fig. 4, this indicates
369 that the decline of the bloom was ongoing in the Labrador basin.

370 POC concentrations and particulate ²³⁴Th activities were moderate to low, except at Station 77 where values were
371 higher in the surface, reaching 11 $\mu\text{mol L}^{-1}$ and 0.45 dpm L^{-1} for the SSF, and, 3.0 $\mu\text{mol L}^{-1}$ and 0.20 dpm L^{-1} for
372 the LSF, respectively. Moderate POC:²³⁴Th ratios were observed in both size fractions, except in the upper layer
373 at station 77 where SSF POC:²³⁴Th ratios were high (Fig. 3). At the Eq depth, POC:²³⁴Th ratios in both size
374 fractions were similar, reached 9.2, 14 and 8.8 $\mu\text{mol dpm}^{-1}$ at Stations 64, 69 and 77, respectively. Interestingly,
375 these ratios are higher than the median ratio determined along the transect.

376 The surface ²³⁴Th/²³⁸U ratios were in the median of those observed along the transect (0.74 ± 0.06 , n=8) with
377 minima of 0.78, 0.66 and 0.73 at Stations 64, 69 and 77, respectively. These ²³⁴Th deficits were nevertheless
378 observed in a relatively shallow layer (Eq depths between 40 and 80 m in this basin; Fig. 2). Stations 64 and 69
379 were also characterized by a low particulate ²³⁴Th activity (combined LSF and SSF) accounting for 10 and 15%
380 of the total ²³⁴Th activity in agreement with relatively low POC concentrations observed at these stations. The
381 ²³⁴Th export flux at Station 64 was slightly greater than those of Stations 69 and 77 but, in general, the ²³⁴Th export
382 fluxes of the Labrador basin were moderate, averaging 758 $\text{dpm m}^{-2} \text{d}^{-1}$ (Table 1). ²³⁴Th scavenging fluxes were
383 also generally low in the Labrador basin, but with again, a slightly lower scavenging flux at Station 64 (Table 1).
384 A higher export ratio was thus estimated at Station 64 (P/J ratio = 0.75), suggesting a more efficient export close
385 to the Greenland margin compared to Stations 69 and 77 (Fig. 6).

386 Below Eq, there was a significant excess of ²³⁴Th relative to ²³⁸U at Stations 69 and 77, reaching respectively 1.08
387 and 1.11. Evidence for shallow remineralisation was also clear from the R100 values exceeding uncertainties
388 (Station 69, $R100=401 \pm 159 \text{ dpm m}^{-2} \text{d}^{-1}$ and Station 77, $R100=252 \pm 165 \text{ dpm m}^{-2} \text{d}^{-1}$, Table 1). The flux
389 reductions due to remineralisation below Eq were 50 and 40% of the fluxes at Eq, respectively.

390 High POC exports were observed within the Labrador basin and in particular at Station 69 where POC export flux
391 reached 10 $\text{mmol m}^{-2} \text{d}^{-1}$. As for the Irminger basin, Puigcorb  et al. (2017) determined a low POC export (0.7
392 $\text{mmol m}^{-2} \text{d}^{-1}$) in May, one month before our sampling period, while Moran et al. (2003) observed higher fluxes
393 reaching 47 $\text{mmol m}^{-2} \text{d}^{-1}$ in July, one month after our sampling period (Fig. 7).

394 4. Discussion

395 In the following section, we first discuss the potential impact of the physics and the non-steady state conditions on
396 the ²³⁴Th export flux estimations. Then, temporal and regional variations of the carbon export fluxes are discussed
397 with regards to the intensity and stage of the bloom, the phytoplankton size structure and the phytoplankton
398 community. Finally, we examine carbon export and transfer efficiencies along the transect.

399 4.1. Validity of the export estimations

400 4.1.1. ²³⁴Th export fluxes under the potential influence of physical conditions

401 The GEOVIDE section sampled a diversity of dynamic regimes (Zunino et al., 2017) including continental margins
402 affected by strong zonal surface currents (LC, WGC and EGC; Mercier et al., 2015; Reverdin et al., 2003), local
403 and seasonal upwelling (close to the Iberian Margin), as well as deep convection zone in the Labrador Sea. In such
404 conditions, Eq. 3, which assumes negligible lateral and vertical advective and diffusive fluxes, may not always be

405 appropriate (Savoie et al., 2006). Whenever possible, we explore quantitatively or qualitatively, the potential
406 errors arising from neglecting physical transport in our calculation.

407 Lateral processes associated with high velocity currents and intense mesoscale activity are known to affect the
408 ^{234}Th distribution (Benitez-Nelson et al., 2000; Resplandy et al., 2012; Roca-Marti et al., 2016b; Savoie et al.,
409 2006). In our case, this may concern several stations located at or close to margins such as Stations 51 and 64,
410 which were respectively subject to the powerful East and West Greenland Currents at the Greenland Margin,
411 Station 77 under influence of the LC on the Newfoundland Margin and Station 1 under influence of the Portugal
412 Current at the Iberian Margin (Fig. 1). However, the impact of the lateral advection cannot be quantified from our
413 dataset, as the possible horizontal gradients of ^{234}Th cannot be resolved at sufficient resolution. As an alternative,
414 we compare stations close to each other such as Stations 44 and 51, both located in the Irminger Basin where
415 surface currents are strong. The Irminger basin in spring is a really patchy and dynamic area (Ceballos-romero et
416 al., 2016; Le Moigne et al., 2012; Puigcorbé et al., 2017) but the relatively high variability of the ^{234}Th fluxes
417 found at these two stations (321 and 922 dpm $\text{m}^{-2} \text{d}^{-1}$, respectively) may also indicate a potential influence of lateral
418 advection. The higher export flux at Station 51 could reflect an input of ^{234}Th depleted waters originating from the
419 Arctic and/or the Greenland shelf. However, Arctic (Cai et al., 2010; Roca-Marti et al., 2016a) and Greenland shelf
420 waters (Station 53, see Table S1) reveal very limited depletions of ^{234}Th relative to ^{238}U . Thus, it is reasonable to
421 consider that the ^{234}Th deficit at Station 51 was essentially driven by vertical rather than horizontal processes.

422 The impact of hydrodynamic processes concerns the open ocean sites, such as stations within the west
423 European and Icelandic basins (Stations 26 and 32) which are subjected to mesoscale activity. An inverse modeling
424 study carried out for the Porcupine Abyssal Plain located in the same region, suggests that the vertical transport of
425 ^{234}Th associated with small-scale structures could represent up to 20% of the estimated vertical export flux
426 (Resplandy et al., 2012). This error is larger than our analytical uncertainty and should be kept in mind when
427 considering the export flux data in this area.

428 In upwelling systems, the contribution of vertical advection on the ^{234}Th distribution has been shown to be
429 important (Buesseler, 1998; Buesseler et al., 1995). Near the Portuguese coast, the intensity of the upwelling is
430 seasonally dependent (Costa Goela et al., 2016; Zúñiga et al., 2016) and was rather inactive at the time of the
431 GEOVIDE cruise (<http://marine.copernicus.eu/>). Therefore, the input of ^{234}Th -rich deep waters to the surface is
432 likely to be limited, as already observed in the northern Iberian margin in early summer (Hall et al., 2000).

433 Downwelling systems, such as the intense convection that occurred in the Labrador basin during the winter prior
434 to our sampling (Kieke and Yashayaev, 2015), are also likely to impact the ^{234}Th distribution. However, a strong
435 vertical advection would homogenize the ^{234}Th activities in the water column, which is not the case during our
436 study (Fig. 2). Therefore, the influence of vertical advection on ^{234}Th export fluxes was neglected.

437 Finally, the contribution of the vertical molecular diffusion estimated using the vertical gradients of total ^{234}Th
438 activity in upper waters and a K_z value ranging between 10^{-4} and $10^{-5} \text{m}^2 \text{s}^{-1}$, as observed in the upper 1000 m
439 between Portugal and Greenland along the OVIDE transect (Ferron et al., 2014). The highest vertical diffusive
440 flux was determined at Station 69 and reached 181 dpm $\text{m}^{-2} \text{d}^{-1}$, which is in the range of the ^{234}Th flux uncertainties.
441 Therefore, the impact of the vertical diffusion has not been considered further.

442 In conclusion, hydrodynamic processes are likely to have at most a limited impact on the measured ^{234}Th export
443 fluxes.

444 4.1.2. Accounting for non-steady state conditions

445 As the cruise sampling scheme did not allow to collect samples through a time series, it was necessary to assume
446 steady state conditions (i.e., no variation of ^{234}Th activity with time). However, as documented in previous studies
447 in the west European and Icelandic basins (Buesseler et al., 1992; Martin et al., 2011), this assumption can be
448 questioned as large variations of ^{234}Th activity were observed at a time scale of one to three weeks along with the
449 onset of the seasonal biological productivity. As a consequence, the SS model was shown to poorly describe the
450 magnitude of the ^{234}Th export flux as it underestimated fluxes by up to a factor of 3 compared to the non-steady
451 state (NSS) model (Buesseler et al., 1992; Martin et al., 2011).

452 During the weeks preceding GEOVIDE, large changes in satellite-derived PP were observed (Fig. 4). In order to
453 evaluate the potential error introduced by the SS approach, we attempted to apply a NSS model (see section 2.3;
454 Eq. 4).

455 The west European and Icelandic basins had the highest NSS ^{234}Th fluxes ($3540 \text{ dpm m}^{-2} \text{ d}^{-1}$ at Station 32) while
456 the Irminger basin had the lowest ($516 \text{ dpm m}^{-2} \text{ d}^{-1}$ at Station 44; Table 1). The NSS ^{234}Th fluxes were either larger
457 or similar to those obtained using the SS model. This results from the fact that the NSS approach used here assumes
458 the observed ^{234}Th activity changes to only reflect a linear decrease from an initial ^{234}Th activity in secular
459 equilibrium with ^{238}U , over the time elapsed since the onset of the bloom (Δt , see section 2.3). For stations sampled
460 shortly after the start of the bloom such as in the Irminger, Icelandic and Labrador basins (Δt ranges from 23 to 43
461 days), the fluxes predicted by the NSS model are from 1.4 to 2.1 fold higher than to the SS fluxes. In the west
462 European and Iberian basins, this difference is reduced (NSS fluxes are from 1.1 to 1.3 fold higher) due to a larger
463 Δt , ranging from 48 to 78 days.

464 As a conclusion, the SS export fluxes may have underestimated ^{234}Th export fluxes at some stations by a maximum
465 factor of 2 such as in the Icelandic basin. Yet, we need to keep in mind that this NSS approach has limitations by
466 assuming the equilibrium between ^{234}Th and ^{238}U at the bloom start and by considering only an increasing deficit
467 of ^{234}Th activity over a given time period (Δt).

468 **4.2. Influence of the intensity and stage of the bloom on POC exports**

469 The GEOVIDE cruise was carried out in late spring (May-June), a period during which the productivity and the
470 carbon export can be important (Sanders et al., 2014). The ^{234}Th proxy integrates the activity deficits over a
471 timescale of several weeks preceding the sampling and it appears thus essential to compare the sampling time in
472 light of the bloom development.

473 Apart from Stations 1 and 13, which were sampled after the bloom, the different basins were sampled during the
474 spring bloom, but at different stages. One of the lowest POC export flux was determined at Station 13 in the Iberian
475 basin, where the intensity of the bloom remained rather low along the season (seasonal VGPM-PP= 81 mmol m^{-2}
476 d^{-1} , Fig. 5) due to oligotrophic conditions (depleted nutrients; Fonseca-Batista et al., 2018). In contrast, the highest
477 POC export flux was determined at Station 1, also in the Iberian basin. Station 1 was sampled after the bloom
478 period and satellite-data showed this station was relatively productive in the early spring ($185 \text{ mmol m}^{-2} \text{ d}^{-1}$ in
479 March, Fig. 4). This greater POC export observed when the bloom had already declined may be caused by an
480 ecosystem change, as already described in the Southern Ocean with the emergence of silicified diatoms because
481 of nutrient stress (e.g., Baines et al., 2010; Claquin et al., 2002).

482 High POC export fluxes were also observed for the west European and Icelandic basins sampled during the bloom.
483 PP appeared maximal just before the sampling in the west European basin (Fig. 4 and 5) and could have promoted
484 these high POC exports. Within the Icelandic basin, both stations were sampled during the productive period,
485 although the peak of the bloom was not yet reached (Fig. 4), suggesting that the export maximum might have
486 occurred later in the season. Both basins have previously been characterized by the presence of fast-sinking
487 particles during the bloom (data from cruises in Spring 2012 and Summer 2009; Villa-Alfageme et al., 2016)
488 promoting the high POC export fluxes.

489 The Irminger basin was sampled close to the bloom maximum, but unlike the west European and Icelandic basins
490 the POC export flux was low there, probably reflecting accumulation of biomass preceding export. Indeed, this
491 area had the highest *in-situ* PP, a high proportion of particulate ^{234}Th in surface waters (reaching 94% of the total
492 ^{234}Th activity at Station 44) and a very low P/J ratio, indicating that ^{234}Th was retained in the upper waters rather
493 than being exported (Fig. 6; Table 1).

494 The Labrador Sea basin was sampled just shortly after the peak of PP and was characterized by low *in-situ* PP,
495 low nutrient concentrations, indicating the beginning of the decline of the bloom. The combination of the important
496 PP a few weeks before our sampling (Fig. 4 and 5) and the decline of the bloom likely triggered the high POC
497 export fluxes, as observed elsewhere (Martin et al., 2011; Roca-Marti et al., 2016b; Stange et al., 2016).

498 Overall, the magnitude of the POC export appears to depend on the degree of progress of the bloom. Indeed, the
499 negative relationship found between the POC export fluxes and the *in-situ* PP relative to the maximal VGPM-PP
500 along the season, representing the bloom stage, highlights that highest export occurs in post bloom periods (Fig.
501 8), as also evidenced from deep sediment trap studies (Lampitt et al., 2010), and is driven by large and rapidly
502 sinking aggregates (Lampitt et al., 2001; Turner and Millward, 2002).

503 **4.3. Influence of the phytoplankton size and community structure on POC exports**

504 In the North Atlantic, the phytoplankton composition varies significantly, depending on the stage of the bloom and
505 on the evolution of environmental parameters such as micro- and macro-nutrient concentrations or stratification
506 depth (Moore et al., 2005). Spatial variations in phytoplankton size structure are known to exert a control on the
507 magnitude of the POC export flux (Boyd and Newton, 1999) and high POC exports are usually related to a greater
508 size of the sinking phytoplankton cells (Alldredge and Silver, 1988; Guidi et al., 2009).

509 Within the Iberian basin, the highest abundance of pico-phytoplankton was observed at Station 13 (Tonnard et al.,
510 in prep.). These conditions are typical of the subtropical and oligotrophic waters (Dortch and Packard, 1989).
511 Villa-Alfageme et al. (2016) highlighted that small cells are usually slow-sinking particles that can be easily
512 remineralised in the upper layers. A small sinking velocity ($<100 \text{ m d}^{-1}$) allows time for bacteria and zooplankton
513 to degrade such particles, thus reducing the export flux. For the same area, Owens et al. (2014) also report a low
514 flux later in October, confirming a lower carbon export in general in this oligotrophic area. However, Station 1
515 was characterized by a greater POC export that could be related to the mixed proportion of micro-, nano- and pico-
516 phytoplankton and thus to the greater proportion of larger cells such as diatoms or haptophytes, increasing the
517 particle sinking velocity. The greater POC export there may also be related to the proximity to the margin, where
518 particle dynamics are intense and lithogenic particles are numerous (Gourain et al., 2018).

519 At higher latitudes, particle sinking velocity has been reported to be high ($>100 \text{ m d}^{-1}$; Villa-Alfageme et al., 2016),
520 as cells generally are of a larger size. Micro-phytoplankton, with dominance of diatoms, represented an important

521 fraction of the phytoplankton community in the west European, Irminger and Labrador basins and the dense
522 frustules of diatoms have been reported to act as ballast for the sinking organic matter (Klaas and Archer, 2002).
523 Fast-sinking particles could have promoted the relatively high POC export fluxes in those basins. However, in the
524 Icelandic basin, the dominance of nano-phytoplankton coincided with relatively high POC export. Both stations
525 in the Icelandic basin were dominated by haptophytes, including coccolithophorids (Tonnard et al., in prep.).
526 Despite their smaller size, the dense calcium carbonate shells of the latter could promote the export of POC
527 (Francois et al., 2002; Lam et al., 2011).
528 Our results suggest that high POC export fluxes can be mediated through either micro- or nano-phytoplankton
529 species, suggesting that sinking velocity is influenced by other parameters than the size, likely their composition
530 and density (Fig. 8).

531 4.4. Export and transfer efficiencies of POC

532 In order to characterize the strength of the biological carbon pump, we used two parameters: the export efficiency
533 (ThE), which is the ratio of the POC export flux at Eq over the PP (Buesseler, 1998) and the transfer efficiency
534 (T100) which is the ratio of the POC export flux at 100 m below Eq over the POC export flux at Eq (Fig. 9). Note
535 that the POC export flux at Eq+100 (Table 3) was calculated by multiplying the ^{234}Th flux at Eq+100 by the POC
536 to ^{234}Th ratio of large particles for the same depth. The POC: ^{234}Th ratio at Eq+100 was deduced from a power law
537 fit (Fig. 3).

538 Based on *in-situ* PP values (Table 3), ThE ranged from 1 (Station 44) to 38% (Station 69) with a median value of
539 7% along the transect. The highest export efficiencies were determined at Stations 1 and 69 with values reaching
540 35 and 38%, respectively. Other stations were characterized by $\text{ThE} \leq 14\%$ with highest values (7 – 14%) at
541 Stations 32, 38, 64 and 77. Export efficiencies around 10% are common in the open ocean (Buesseler, 1998). A
542 lower export efficiency can be related to important microbial and zooplankton grazing activities or to biomass
543 accumulation in surface waters (Planchon et al., 2013, 2015). A high ThE can result from many factors such as the
544 presence of large and/or dense and fast sinking particles, low surface remineralisation, active zooplankton
545 migration or nutrient stress (Ceballos-romero et al., 2016; Le Moigne et al., 2016; Planchon et al., 2013).
546 Interestingly, stations with the highest ThE were also characterized by the lowest PP (Stations 1 and 69) while
547 stations with the lowest ThE were characterized by the highest PP (Stations 44 and 51). This inverse relationship
548 between PP and ThE was significant for all stations of the GEOVIDE cruise (regression slope: -0.20; $r^2=0.58$;
549 $p<0.01$; $n=11$; Fig. S2) and has been explained in the Southern Ocean by the temporal decoupling between PP and
550 export due to biomass accumulation in surface waters (Henson et al., 2015; Planchon et al., 2013) as well as by
551 other processes such as zooplankton grazing and bacterial activity (Maiti et al., 2013; Le Moigne et al., 2016;
552 Roca-Marti et al., 2016a). Such particle recycling has been also observed in the North Atlantic (Collins et al.,
553 2015; Giering et al., 2014; Marsay et al., 2015) limiting POC export to the deep ocean. A recent study in the
554 Icelandic and Irminger basins highlights the impact of the bloom dynamics on the particle export efficiency
555 resulting in strong seasonal variability of the ThE (Ceballos-Romero et al., 2016). Our estimates are generally in
556 the lower range of export efficiencies reported by others for the North Atlantic with values ranging from 1 to 42%
557 in the western European basin (Buesseler et al., 1992; Lampitt et al., 2008; Thomalla et al., 2008), from 5 to 8%
558 in the Icelandic basin (Ceballos-romero et al., 2016), from 4 to 16% in the Irminger basin (Ceballos-romero et al.,
559 2016) and from 4 to > 100% in the Labrador basin (Moran et al., 2003). This wide range confirms that export

560 efficiencies are highly variable in the North Atlantic during the period of our study. The overall low export
561 efficiency of the North Atlantic is characteristic of highly productive areas of the world ocean.


562 However, it should be kept in mind that the ThE calculation is based on two parameters that are integrating
563 processes over different time scales: 24 h for *in-situ* PP and several weeks for export. Strong variability of PP in
564 short time period could therefore have a strong impact on the outcome. Therefore, ThE ratios were also estimated
565 using the VGPM-derived 8-day, 32-day and seasonal PP (Table 3). As seen in Section 2.7, there are no significant
566 differences between the VGPM-PP estimates regardless of the integrations times, and thus no significant
567 differences between the corresponding ThE values. Stations 1 and 69 are exceptions with ThE values decreasing
568 from 35 to 12% and from 38 to 8%, respectively, due to unusually low *in-situ* PP during our study which led to
569 over-estimated ThE.

570 Carbon transfer efficiencies (T100) ranged from 30 (Station 69) to 78% (Station 32). Generally, the fluxes at these
571 greater depths were characterized by greater error bars (see Fig. 9) due to the increasing uncertainty of the ^{234}Th
572 fluxes with increasing depth. The highest T100 were observed within the Icelandic basin with values reaching 78
573 and 74% at Stations 32 and 38 respectively. On the contrary, the lowest T100 values were observed at Stations 1,
574 13, 21 and 69 (between 30 and 49%) highlighting greater carbon remineralisation between Eq and Eq+100 m at
575 these latter stations, as well as confirming important regional variability of the transfer efficiency as reported also
576 by others (Lam et al., 2011; Lutz et al., 2002). The low T100 (and high R100) values observed in the eastern part
577 of the transect (Stations 1, 13 and, to a lesser extent Station 21) likely reflect an important bacterial activity in
578 these warmer waters (>13°C in the upper 100 m; Iversen and Ploug, 2013; Marsay et al., 2015; Rivkin and
579 Legendre, 2001). This efficient recycling is characteristic for regeneration-based microbial food webs in
580 oligotrophic regimes (Karl, 1999; Thomalla et al., 2006). In the Icelandic basin, the high T100 may be related to
581 the large abundance of coccolithophorids (Tonnard et al., in prep.) known to enhance the POC transfer due to their
582 ballasting effect (Francois et al., 2002; Lam et al., 2011). Indeed, Bach et al. (2016) found that a bloom of
583 coccolithophorids can increase the transfer efficiency through the mesopelagic layer by 14-24%. Finally, the
584 Labrador and Irminger basins exhibit relatively similar T100 (between 50 and 69%), except at Station 69 where
585 the lowest T100 was observed. This is also in agreement with the highest R100 and carbon remineralisation flux
586 determined with the Ba_{xs} proxy (Lemaitre et al., 2018). The central Labrador basin, in proximity of Station 69, was
587 characterized by strong subduction of the LSW during the winter preceding the GEOVIDE cruise. This
588 downwelling could have promoted an important organic matter export leading to important prokaryotic
589 heterotrophic activity in mesopelagic waters. This enhanced remineralisation was still observed during GEOVIDE
590 as traced by a large mesopelagic Ba_{xs} content (Lemaitre et al., 2018).

591 5. Conclusion

592 Overall, POC export varied by a factor of ~ 9 along the transect highlighting an important spatial variation. POC
593 flux results obtained from other studies in the North Atlantic range from similar to up to 27 times larger values,
594 with rapid changes over month, confirming the large temporal variability of the POC export fluxes.

595 The magnitude of the POC export seems to be associated with the state of the bloom. Accumulation of biomass in
596 surface waters during the bloom may induce a limitation of the POC export flux while during the post bloom
597 period increasing numbers of rapidly sinking particles increases POC export.

598 The magnitude of the fluxes seems also to be ed to the phytoplankton size and community structure. One of
599 the lowest POC export fluxes was found at the stations where pico-phytoplankton dominated the community. In
600 contrast, the areas composed by micro- and nano-phytoplankton were characterized by high POC export fluxes.
601 These areas were dominated by diatoms or coccolithophorids, known to strongly ballast the POC export fluxes.
602 This suggests that the size as well as the composition and density of the particles likely play an important role on
603 the particulate sinking velocities and thus on the magnitude of the POC export fluxes.
604 For most stations, the fraction of primary production that is exported from the surface zone (export efficiency) was
605 $\leq 14\%$, which is in agreement with the global ocean export efficiency ($\sim 10\%$; Buesseler, 1998). Export efficiency
606 was also inversely related to primary production, indicating that the North Atlantic during our study behaved like
607 most of the highly productive areas of the world's ocean, with a low export efficiency. Finally, the fraction of POC
608 that is not remineralised in the mesopelagic zone (transfer efficiency) fits within the range of measured transfer
609 efficiencies reported elsewhere (e.g., Black et al., 2017; Buesseler and Boyd, 2009). The highest transfer
610 efficiencies were determined at the stations where coccolithophorids dominated.

611 **Acknowledgements**

612 We would like to thank the captain and the crew of the R/V Pourquoi Pas?, the chief scientists Pascale Lherminier
613 and Géraldine Sarthou, as well as Fabien Perault and Emmanuel De Saint Léger (CNRS DT-INSU), Pierre
614 Branellec, Michel Hamon, Catherine Kermabon, Philippe Le Bot, Stéphane Leizour and Olivier Ménage
615 (Laboratoire d'Océanographie Physique et Spatiale) for their technical expertise during ISP and CTD deployments
616 and Catherine Schmechtig for the GEOVIDE database management. We also acknowledge Emilie Grossteffan,
617 Manon Le Goff, Morgane Galinari and Paul Tréguer for the analysis of nutrients. Special thanks to Maxi Castrillejo
618 (UAB, Spain), Catherine Jeandel (LEGOS, France), Virginie Sanial (WHOI, USA), Raphaëlle Sauzède (LOV,
619 France) and Lorna Foliot (LSCE, France) for their help at sea and for the ISP coordination. We would also like to
620 thank Phoebe Lam for providing two modified McLane ISP. Laurence Monin (MRAC, Belgium), David
621 Verstraeten, Claire Mourgues and Martine Leermarkers (VUB, Belgium) greatly helped during sample processing
622 and element analysis by ICP-MS and EA-IRMS. Audrey Plante (ULB, Belgium) and Emilie Le Roy (LEGOS,
623 France) assisted with the counting of the residual Thorium-234 activities. Satellite primary production data and
624 visualizations used in this study were produced with the Ocean Productivity website at Oregon State University.
625 This work was funded by the Flanders Research Foundation (project G071512N), the Vrije Universiteit Brussel
626 (Strategic Research Program, project SRP-2), the French ANR Blanc GEOVIDE (ANR-13-BS06-0014), ANR
627 RPDOC BITMAP (ANR-12-PDOC-0025-01), IFREMER, CNRS-INSU (programme LEFE), INSU OPTIMISP
628 and Labex-Mer (ANR-10-LABX-19).

629 **References**

- 630 Alldredge, A. L. and Silver, M. W.: Characteristics, dynamics and significance of marine snow, *Prog. Oceanogr.*,
631 20, 41–82, 1988.
- 632 Aminot, A. and Kérouel, R.: Dosage automatique des nutriments dans les eaux marines: méthodes en flux continu,
633 Ifremer-Qu., 2007.
- 634 Bach, L. T., Boxhammer, T., Larsen, A., Hildebrandt, N., Schulz, K. G. and Riebesell, U.: Influence of plankton

- 635 community structure on the sinking velocity of marine aggregates, *Global Biogeochem. Cycles*, 30, 1145–1165,
636 doi:10.1002/2016GB005372, 2016.
- 637 Baines, S. B., Twining, B. S., Brzezinski, M. A., Nelson, D. M. and Fisher, N. S.: Causes and biogeochemical
638 implications of regional differences in silicification of marine diatoms, *Global Biogeochem. Cycles*, 24(4), 1–15,
639 doi:10.1029/2010GB003856, 2010.
- 640 Behrenfeld, M. and Falkowski, P. G.: A consumer's guide to phytoplankton primary productivity models, *Limnol.*
641 *Oceanogr.*, 42(7), 1479–1491, doi:10.4319/lo.1997.42.7.1479, 1997.
- 642 Behrenfeld, M. J., Boss, E., Siegel, D. A. and Shea, D. M.: Carbon-based ocean productivity and phytoplankton
643 physiology from space, *Global Biogeochem. Cycles*, 19(1), 1–14, doi:10.1029/2004GB002299, 2005.
- 644 Benitez-Nelson, C. R., Buesseler, K. O. and Crossin, G.: Upper ocean carbon export, horizontal transport, and
645 vertical eddy diffusivity in the southwestern Gulf of Maine, *Cont. Shelf Res.*, 20(6), 707–736, doi:10.1016/S0278-
646 4343(99)00093-X, 2000.
- 647 Bhat, S. G., Krishnaswanmy, S., Lal, D. and Moore, W. S.: $^{234}\text{Th}/^{238}\text{U}$ Ratios in the Ocean, *Earth Planet. Sci.*
648 *Lett.*, 5, 433–491, 1969.
- 649 Black, E. E., Buesseler, K. O., Pike, S. M. and Lam, P. J.: ^{234}Th as a tracer of particulate export and
650 remineralization in the southeastern tropical Pacific, *Mar. Chem.*, (June), 1–16,
651 doi:10.1016/j.marchem.2017.06.009, 2017.
- 652 Boyd, P. W. and Newton, P. P.: Does planktonic community structure determine downward particulate organic
653 carbon flux in different oceanic provinces?, *Deep Sea Res. Part I Oceanogr. Res. Pap.*, 46, 63–91, 1999.
- 654 Buesseler, K. O.: The decoupling of production and particulate export in the surface ocean, *Global Biogeochem.*
655 *Cycles*, 12(2), 297, doi:10.1029/97GB03366, 1998.
- 656 Buesseler, K. O. and Boyd, P. W.: Shedding light on processes that control particle export and flux attenuation in
657 the twilight zone of the open ocean, *Limnol. Oceanogr.*, 54(4), 1210–1232, doi:10.4319/lo.2009.54.4.1210, 2009.
- 658 Buesseler, K. O., Bacon, M. P., Kirk Cochran, J. and Livingston, H. D.: Carbon and nitrogen export during the
659 JGOFS North Atlantic Bloom experiment estimated from ^{234}Th : ^{238}U disequilibria, *Deep Sea Res. Part A.*
660 *Oceanogr. Res. Pap.*, 39(7–8), 1115–1137, doi:10.1016/0198-0149(92)90060-7, 1992.
- 661 Buesseler, K. O., Andrews, J. A., Hartman, M. C., Belastock, R. and Chai, F.: Regional estimates of the export
662 flux of particulate organic carbon derived from thorium-234 during the JGOFS EqPac program, *Deep Sea Res.*
663 *Part II Top. Stud. Oceanogr.*, 42(2–3), 777–804, doi:10.1016/0967-0645(95)00043-P, 1995.
- 664 Buesseler, K. O., Benitez-Nelson, C. R., Moran, S. B., Burd, a., Charette, M., Cochran, J. K., Coppola, L., Fisher,
665 N. S., Fowler, S. W., Gardner, W. D., Guo, L. D., Gustafsson, Ö., Lamborg, C., Masque, P., Miquel, J. C., Passow,
666 U., Santschi, P. H., Savoye, N., Stewart, G. and Trull, T.: An assessment of particulate organic carbon to thorium-
667 ^{234}Th ratios in the ocean and their impact on the application of ^{234}Th as a POC flux proxy, *Mar. Chem.*, 100(3–4
668 SPEC. ISS.), 213–233, doi:10.1016/j.marchem.2005.10.013, 2006.
- 669 Buesseler, K. O., Trull, T. W., Steinberg, D. K., Silver, M. W., Siegel, D. a., Saitoh, S. I., Lamborg, C. H., Lam,
670 P. J., Karl, D. M., Jiao, N. Z., Honda, M. C., Elskens, M., Dehairs, F., Brown, S. L., Boyd, P. W., Bishop, J. K. B.
671 and Bidigare, R. R.: VERTIGO (VERTical Transport In the Global Ocean): A study of particle sources and flux
672 attenuation in the North Pacific, *Deep Sea Res. Part II Top. Stud. Oceanogr.*, 55(14–15), 1522–1539,
673 doi:10.1016/j.dsr2.2008.04.024, 2008.
- 674 Cai, P., Rutgers Van Der Loeff, M., Stimac, I., Nthig, E. M., Lepore, K. and Moran, S. B.: Low export flux of
675 particulate organic carbon in the central Arctic Ocean as revealed by ^{234}Th : ^{238}U disequilibrium, *J. Geophys.*
676 *Res. Ocean.*, 115(10), 1–21, doi:10.1029/2009JC005595, 2010.
- 677 Ceballos-romero, E., Le Moigne, F. A. C., Henson, S., Marsay, C. M., Sanders, R. J., García-Tenorio, R. and Villa-
678 Alfageme, M.: Influence of bloom dynamics on particle export efficiency in the North Atlantic: a comparative
679 study of radioanalytical techniques and sediment traps, *Mar. Chem.*, 186, 198–210,
680 doi:10.1016/j.marchem.2016.10.001, 2016.

- 681 Claquin, P., Martin-Jézéquel, V., Kromkamp, J. C., Veldhuis, M. J. W. and Kraay, G. W.: Uncoupling of silicon
682 compared with carbon and nitrogen metabolisms and the role of the cell cycle in continuous cultures of
683 *Thalassiosira pseudonana* (Bacillariophyceae) under light, nitrogen, and phosphorus control, *J. Phycol.*, 38(5),
684 922–930, doi:10.1046/j.1529-8817.2002.t01-1-01220.x, 2002.
- 685 Coale, K. H. and Bruland, K. W.: Thorium-234:uranium-238 disequilibria within the California Current, *Limnol.*
686 *Oceanogr.*, 30(1), 22–33, doi:10.4319/lo.1985.30.1.0022, 1985.
- 687 Cochran, J. K. and Masqué, P.: Short-lived U/Th series radionuclides in the ocean: Tracers for scavenging rates,
688 export fluxes and particle dynamics, *Rev. Mineral. Geochemistry*, 52, 461–492, doi:10.2113/0520461, 2003.
- 689 Collins, J. R., Edwards, B. R., Thamatrakoln, K., Ossolinski, J. E., Ditullio, G. R., Bidle, K. D., Doney, S. C. and
690 Mooy, B. A. S. Van: The multiple fates of sinking particles in the North Atlantic Ocean, *Global Biogeochem.*
691 *Cycles*, 29, 1471–1494, doi:10.1002/2014GB005037, 2015.
- 692 Costa Goela, P., Cordeiro, C., Danchenko, S., Icelly, J., Cristina, S. and Newton, A.: Time series analysis of data
693 for sea surface temperature and upwelling components from the southwest coast of Portugal, *J. Mar. Syst.*, 163,
694 12–22, doi:10.1016/j.jmarsys.2016.06.002, 2016.
- 695 Dortch, Q. and Packard, T. T.: Differences in biomass structure between oligotrophic and eutrophic marine
696 ecosystems, *Deep Sea Res. Part A. Oceanogr. Res. Pap.*, 36(2), 223–240, 1989.
- 697 Eppley, R. W.: Temperature and phytoplankton growth in the sea, *Fish. Bull.*, 70(4), 1063–1085, 1972.
- 698 Esaias, W. E., Feldman, G. C., MnClain, C. R. and Elrod, J. A.: Monthly satellite-derived phytoplankton pigment
699 distribution for the North Atlantic basin, *Oceanography Rep.*, 67(44), 835–837, 1986.
- 700 Ferron, B., Kokoszka, F., Mercier, H. and Lherminier, P.: Dissipation rate estimates from microstructure and
701 finescale internal wave observations along the A25 Greenland-Portugal OVIDE line, *J. Atmos. Ocean. Technol.*,
702 31(11), 2530–2543, doi:10.1175/JTECH-D-14-00036.1, 2014.
- 703 Fonseca-Batista, D., Li, X., Riou, V., Michotey, V., Fripiat, F., Deman, F., Guasco, S., Brion, N., Lemaitre, N.,
704 Planchon, F., Tonnard, M., Planquette, H., Gallinari, M., Sarthou, G., Elskens, M., Chou, L. and Dehairs, F.:
705 Evidence of high N₂ fixation rates in productive waters of the temperate Northeast Atlantic, *Biogeosciences*, 2018.
- 706 Francois, R., Honjo, S., Krishfield, R. and Manganini, S.: Factors controlling the flux of organic carbon to the
707 bathypelagic zone of the ocean, *Global Biogeochem. Cycles*, 16(4), 1–20, doi:10.1029/2001GB001722, 2002.
- 708 GEOTRACES: GEOTRACES (an international study of the marine biogeochemical cycle of trace elements and
709 isotopes): *Science Plan.*, 2006.
- 710 Giering, S. L. C., Sanders, R., Lampitt, R. S., Anderson, T. R., Tamburini, C., Boutrif, M., Zubkov, M. V, Marsay,
711 C. M., Henson, S. A., Saw, K., Cook, K. and Mayor, D. J.: Reconciliation of the carbon budget in the ocean's
712 twilight zone, *Nature*, 507(7493), 480–483, doi:10.1038/nature13123, 2014.
- 713 Giering, S. L. C., Sanders, R., Martin, A. P., Lindemann, C., Möller, K. O., Daniels, C. J., Mayor, D. J. and St.
714 John, M. A.: High export via small particles before the onset of the North Atlantic spring bloom, *J. Geophys. Res.*,
715 121, 1–17, doi:10.1002/2016JC012048.Received, 2016.
- 716 Gourain, A., Planquette, H., Cheize, M., Menzel, J.-L., Boutorh, J., Shelley, R., Pereira Contraira, L., Lemaitre,
717 N., Lacan, F., Lherminier, P. and Sarthou, G.: Particulate trace metals along the GEOVIDE section,
718 *Biogeosciences*, 2018.
- 719 Guidi, L., Stemmann, L., Jackson, G. A., Ibanez, F., Claustre, H., Legendre, L., Picheral, M. and Gorsky, G.:
720 Effects of phytoplankton community on production, size and export of large aggregates: A world-ocean analysis,
721 *Limnol. Oceanogr.*, 54(6), 1951–1963, 2009.
- 722 Guidi, L., Legendre, L., Reygondeau, G., Uitz, J., Stemmann, L. and Henson, S. A.: A new look at ocean carbon
723 remineralization for estimating deepwater sequestration, *Glob. Planet. Change*, 29, 1044–1059,
724 doi:10.1002/2014GB005063.Received, 2015.
- 725 Hall, I. R., Schmidt, S., McCave, I. N. and Reyss, J. L.: Particulate matter distribution and ²³⁴Th/²³⁸U
726 disequilibrium along the Northern Iberian Margin: implications for particulate organic carbon export, *Deep. Res.*

- 727 Part I, 47, 557–582, 2000.
- 728 Hama, T., Miyazaki, T., Ogawa, Y., Iwakuma, T., Takahashi, M., Otsuki, A. and Ichimura, S.: Measurement of
729 photosynthetic production of a marine phytoplankton population using a stable ¹³C isotope, *Mar. Biol.*, 73, 31–36,
730 1983.
- 731 Henson, S. A., Dunne, J. P. and Sarmiento, J. L.: Decadal variability in North Atlantic phytoplankton blooms, *J.*
732 *Geophys. Res.*, 114(C4), C04013–C04013, doi:10.1029/2008JC005139, 2009.
- 733 Henson, S. A., Sanders, R. and Madsen, E.: Global patterns in efficiency of particulate organic carbon export and
734 transfer to the deep ocean, *Global Biogeochem. Cycles*, 26(1), 1–14, doi:10.1029/2011GB004099, 2012.
- 735 Henson, S. A., Yool, A. and Sanders, R.: Variability in efficiency of particulate organic carbon export: a model
736 study, *Global Biogeochem. Cycles*, 29, 33–45, doi:10.1002/2014GB004965. Received, 2015.
- 737 Herndl, G. J. and Reinthaler, T.: Microbial control of the dark end of the biological pump, *Nat. Geosci.*, 6(9), 718–
738 724, doi:10.1038/ngeo1921, 2013.
- 739 Honjo, S. and Manganini, S. J.: Annual biogenic particle fluxes to the interior of the North Atlantic Ocean; studied
740 at 34°N 21°W and 48°N 21°W, *Deep Sea Res. Part I Oceanogr. Res. Pap.*, 40(1), 587–607, 1993.
- 741 Iversen, M. H. and Ploug, H.: Temperature effects on carbon-specific respiration rate and sinking velocity of
742 diatom aggregates – potential implications for deep ocean export processes, *Biogeosciences*, 10, 4073–4085,
743 doi:10.5194/bg-10-4073-2013, 2013.
- 744 Karl, D. M.: A Sea of change: Biogeochemical variability in the North Pacific Subtropical Gyre, *Ecosystems*, 2,
745 181–214, 1999.
- 746 Kieke, D. and Yashayaev, I.: Studies of Labrador Sea Water formation and variability in the subpolar North
747 Atlantic in the light of international partnership and collaboration, *Prog. Oceanogr.*, 132, 220–232,
748 doi:10.1016/j.pocean.2014.12.010, 2015.
- 749 Klaas, C. and Archer, D. E.: Association of sinking organic matter with various types of mineral ballast in the deep
750 sea: Implications for the rain ratio, *Global Biogeochem. Cycles*, 16(4), 1–14, doi:10.1029/2001GB001765, 2002.
- 751 Lam, P. J., Doney, S. C. and Bishop, J. K. B.: The dynamic ocean biological pump: Insights from a global
752 compilation of particulate organic carbon, CaCO₃, and opal concentration profiles from the mesopelagic, *Global*
753 *Biogeochem. Cycles*, 25(3), 1–14, doi:10.1029/2010GB003868, 2011.
- 754 Lampitt, R. S., Bett, B. J., Kiriakoulakis, K., Popova, E. E., Ragueneau, O., Vangriesheim, A. and Wolff, G. A.:
755 Material supply to the abyssal seafloor in the Northeast Atlantic, *Prog. Oceanogr.*, 50, 27–63, 2001.
- 756 Lampitt, R. S., Boorman, B., Brown, L., Lucas, M., Salter, I., Sanders, R., Saw, K., Seeyave, S., Thomalla, S. J.
757 and Turnewitsch, R.: Particle export from the euphotic zone: Estimates using a novel drifting sediment trap, 234Th
758 and new production, *Deep Sea Res. Part I Oceanogr. Res. Pap.*, 55(11), 1484–1502, doi:10.1016/j.dsr.2008.07.002,
759 2008.
- 760 Lampitt, R. S., Salter, I., de Cuevas, B. A., Hartman, S., Larkin, K. E. and Pebody, C. A.: Long-term variability of
761 downward particle flux in the deep northeast Atlantic: Causes and trends, *Deep Sea Res. Part II Top. Stud.*
762 *Oceanogr.*, 57(15), 1346–1361, doi:10.1016/j.dsr2.2010.01.011, 2010.
- 763 Lemaitre, N., Planquette, H., Planchon, F., Sarthou, G., Jacquet, S., García-Ibáñez, M. I., Gourain, A., Cheize, M.,
764 Monin, L., André, L., Laha, P., Terry, H. and Dehairs, F.: Particulate barium tracing significant mesopelagic
765 carbon remineralisation in the North Atlantic, *Biogeosciences*, 2018.
- 766 Lemaitre, N., Planquette, H., Planchon, F., Dehairs, F., Roig, S. and Sarthou, G.: High variability of export fluxes
767 along the North Atlantic GEOTRACES section GA01: Importance of minerals as ballast of particulate organic
768 carbon export., in prep., n.d.
- 769 Lima, I. D., Lam, P. J. and Doney, S. C.: Dynamics of particulate organic carbon flux in a global ocean model,
770 *Biogeosciences*, 11(4), 1177–1198, doi:10.5194/bg-11-1177-2014, 2014.
- 771 Longhurst, A. R.: *Ecological geography of the sea*, Academic P., San Diego., 2010.

- 772 Lutz, M., Dunbar, R. and Caldeira, K.: Regional variability in the vertical flux of particulate organic carbon in the
773 ocean interior, *Global Biogeochem. Cycles*, 16(3), 1–15, doi:10.1029/2000GB001383, 2002.
- 774 Maiti, K., Benitez-Nelson, C. R. and Buesseler, K. O.: Insights into particle formation and remineralization using
775 the short-lived radionuclide, Thorium-234, *Geophys. Res. Lett.*, 37(May), 2–7, doi:10.1029/2010GL044063, 2010.
- 776 Maiti, K., Charette, M. A., Buesseler, K. O. and Kahru, M.: An inverse relationship between production and export
777 efficiency in the Southern Ocean, *Geophys. Res. Lett.*, 40(8), 1557–1561, doi:10.1002/grl.50219, 2013.
- 778 Marsay, C. M., Sanders, R. J., Henson, S. A., Pabortsava, K., Achterberg, E. P. and Lampitt, R. S.: Attenuation of
779 sinking particulate organic carbon flux through the mesopelagic ocean., *Proc. Natl. Acad. Sci. U. S. A.*, 112(4),
780 1089–1094, doi:10.1073/pnas.1415311112, 2015.
- 781 Martin, P., Lampitt, R. S., Jane Perry, M., Sanders, R., Lee, C. and D'Asaro, E.: Export and mesopelagic particle
782 flux during a North Atlantic spring diatom bloom, *Deep Sea Res. Part I Oceanogr. Res. Pap.*, 58(4), 338–349,
783 doi:10.1016/j.dsr.2011.01.006, 2011.
- 784 Mercier, H., Lherminier, P., Sarafanov, A., Gaillard, F., Daniault, N., Desbruyères, D., Falina, A., Ferron, B.,
785 Gourcuff, C., Huck, T. and Thierry, V.: Variability of the meridional overturning circulation at the Greenland-
786 Portugal OVIDE section from 1993 to 2010, *Prog. Oceanogr.*, 132, 250–261, doi:10.1016/j.pocean.2013.11.001,
787 2015.
- 788 Le Moigne, F. A. C., Sanders, R. J., Villa-Alfageme, M., Martin, A. P., Pabortsava, K., Planquette, H., Morris, P.
789 J. and Thomalla, S. J.: On the proportion of ballast versus non-ballast associated carbon export in the surface
790 ocean, *Geophys. Res. Lett.*, 39(15–16), L15610–L15610, doi:10.1029/2012GL052980, 2012.
- 791 Le Moigne, F. A. C., Villa-Alfageme, M., Sanders, R. J., Marsay, C., Henson, S. and García-Tenorio, R.: Export
792 of organic carbon and biominerals derived from ²³⁴Th and ²¹⁰Po at the Porcupine Abyssal Plain, *Deep Sea Res.
793 Part I Oceanogr. Res. Pap.*, 72(August), 88–101, doi:10.1016/j.dsr.2012.10.010, 2013a.
- 794 Le Moigne, F. A. C., Henson, S. A., Sanders, R. J. and Madsen, E.: Global database of surface ocean particulate
795 organic carbon export fluxes diagnosed from the ²³⁴Th technique, *Earth Syst. Sci. Data*, 5(2), 295–304,
796 doi:10.5194/essd-5-295-2013, 2013b.
- 797 Le Moigne, F. A. C., Henson, S. A., Cavan, E. L., Georges, C., Pabortsava, K., Achterberg, E. P., Ceballos-romero,
798 E. and Zubkov, M.: What causes the inverse relationship between primary production and export efficiency in the
799 Southern Ocean?, *Geophys. Res. Lett.*, 43, 1–10, doi:10.1002/2016GL068480.Received, 2016.
- 800 Moore, C. M., Lucas, M. I., Sanders, R. and Davidson, R.: Basin-scale variability of phytoplankton bio-optical
801 characteristics in relation to bloom state and community structure in the Northeast Atlantic, *Deep Sea Res. Part I
802 Oceanogr. Res. Pap.*, 52, 401–419, doi:10.1016/j.dsr.2004.09.003, 2005.
- 803 Moore, C. M., Mills, M. M., Langlois, R., Milne, A., Achterberg, E. P., Roche, J. La and Geider, R. J.: Relative
804 influence of nitrogen and phosphorus availability on phytoplankton physiology and productivity in the oligotrophic
805 sub-tropical North Atlantic Ocean, *Limnol. Oceanogr.*, 53(1), 291–305, 2008.
- 806 Moran, S. B., Weinstein, S. E., Edmonds, H. N., Smith, J. N., Kelly, R. P., Pilson, M. E. Q. and Harrison, W. G.:
807 Does ²³⁴Th/²³⁸U disequilibrium provide an accurate record of the export flux of particulate organic carbon from
808 the upper ocean?, *Limnol. Oceanogr.*, 48(3), 1018–1029, doi:10.4319/lo.2003.48.3.1018, 2003.
- 809 Mouw, C. B., Barnett, A., Mckinley, G. A., Gloege, L. and Pilcher, D.: Phytoplankton size impact on export flux
810 in the global Ocean, *Global Biogeochem. Cycles*, 30, 1542–1562, doi:10.1002/2015GB005355, 2016.
- 811 Owens, S. A., Buesseler, K. O. and Sims, K. W. W.: Re-evaluating the ²³⁸U-salinity relationship in seawater:
812 Implications for the ²³⁸U-²³⁴Th disequilibrium method, *Mar. Chem.*, 127(1–4), 31–39,
813 doi:10.1016/j.marchem.2011.07.005, 2011.
- 814 Owens, S. A., Pike, S. and Buesseler, K. O.: Thorium-234 as a tracer of particle dynamics and upper ocean export
815 in the Atlantic Ocean, *Deep Sea Res. Part II Top. Stud. Oceanogr.*, 116, 42–59, doi:10.1016/j.dsr2.2014.11.010,
816 2014.
- 817 Pike, S., Buesseler, K. O., Andrews, J. and Savoye, N.: Quantification of ²³⁴Th recovery in small volume seawater

- 818 samples by Inductively Coupled Plasma Mass Spectrometry, *J. Radioanal. Nucl. Chem.*, 263, 355–360, 2005.
- 819 Planchon, F., Cavagna, A.-J., Cardinal, D., André, L. and Dehairs, F.: Late summer particulate organic carbon
820 export and twilight zone remineralisation in the Atlantic sector of the Southern Ocean, *Biogeosciences*, 10(2),
821 803–820, doi:10.5194/bg-10-803-2013, 2013.
- 822 Planchon, F., Ballas, D., Cavagna, A.-J., Bowie, A. R., Davies, D. M., Trull, T., Laurenceau, E. C., van der Merwe,
823 P. and Dehairs, F.: Carbon export in the naturally iron-fertilized Kerguelen area of the Southern Ocean based on
824 the ²³⁴Th approach, *Biogeosciences*, 12, 3831–3848, doi:10.5194/bg-12-3831-2015, 2015.
- 825 Puigcorbé, V., Roca-Martí, M., Masqué, P., Benitez-Nelson, C., Rutgers van der Loeff, M., Bracher, A. and
826 Moreau, S.: Latitudinal distributions of particulate carbon export across the North Western Atlantic Ocean, *Deep
827 Sea Res. Part I Oceanogr. Res. Pap.*, doi:10.1016/j.dsr.2017.08.016, 2017.
- 828 Ras, J., Claustre, H. and Uitz, J.: Spatial variability of phytoplankton pigment distributions in the Subtropical South
829 Pacific Ocean: comparison between in situ and predicted data, *Biogeosciences*, 5, 353–369, 2008.
- 830 Resplandy, L., Martin, A. P., Le Moigne, F., Martin, P., Aquilina, A., M??mery, L., L??vy, M. and Sanders, R.:
831 How does dynamical spatial variability impact ²³⁴Th-derived estimates of organic export?, *Deep Sea Res. Part I
832 Oceanogr. Res. Pap.*, 68, 24–45, doi:10.1016/j.dsr.2012.05.015, 2012.
- 833 Reverdin, G., Niiler, P. P. and Valdimarsson, H.: North Atlantic Ocean surface currents, *J. Geophys. Res.*, 108, 1–
834 21, doi:10.1029/2001JC001020, 2003.
- 835 Riley, G.: Phytoplankton of the North Central Sargasso Sea, 1950-52, *Limnol. Oceanogr.*, 2, 252–270,
836 doi:10.1002/lno.1957.2.3.0252, 1957.
- 837 Rivkin, R. B. and Legendre, L.: Biogenic carbon cycling in the upper ocean: Effects of microbial respiration,
838 *Science (80-.)*, 291, 2398–2400, 2001.
- 839 Roca-Marti, M., Puigcorbé, V., van der Loeff, M. R., Katlein, C., Fernandez-Mendez, M., Peeken, I. and Masqué,
840 P.: Carbon export fluxes and export efficiency in the central Arctic during the record sea-ice minimum in 2012: a
841 joint ²³⁴Th/²³⁸U and ²¹⁰Po/²¹⁰Pb study, *J. Geophys. Res.*, 121, 1–20, doi:10.1002/2016JC011816.Received,
842 2016a.
- 843 Roca-Marti, M., Puigcorbé, V., Iversen, M. H., van der Loeff, M. R., Klaas, C., Cheah, W., Bracher, A. and
844 Masqué, P.: High particulate organic carbon export during the decline of a vast diatom bloom in the Atlantic sector
845 of the Southern Ocean, *Deep Sea Res. Part II Top. Stud. Oceanogr.*, doi:10.1016/j.dsr2.2015.12.007, 2016b.
- 846 Rutgers van der Loeff, M., Cai, P. H., Stimac, I., Bracher, A., Middag, R., Klunder, M. B. and van Heuven, S. M.
847 A. C.: ²³⁴Th in surface waters: Distribution of particle export flux across the Antarctic Circumpolar Current and
848 in the Weddell Sea during the GEOTRACES expedition ZERO and DRAKE, *Deep. Res. Part II Top. Stud.
849 Oceanogr.*, 58(25–26), 2749–2766, doi:10.1016/j.dsr2.2011.02.004, 2011.
- 850 Rutgers van der Loeff, M. M., Sarin, M. M., Baskaran, M., Benitez-Nelson, C., Buesseler, K. O., Charette, M.,
851 Dai, M., Gustafsson, Ö., Masque, P., Morris, P. J., Orlandini, K., Rodriguez y Baena, A., Savoye, N., Schmidt, S.,
852 Turnewitsch, R., Vöge, I. and Waples, J. T.: A review of present techniques and methodological advances in
853 analyzing ²³⁴Th in aquatic systems, *Mar. Chem.*, 100(3–4 SPEC. ISS.), 190–212,
854 doi:10.1016/j.marchem.2005.10.012, 2006.
- 855 Sanders, R., Morris, P. J., Poulton, A. J., Stinchcombe, M. C., Charalampopoulou, A., Lucas, M. I. and Thomalla,
856 S. J.: Does a ballast effect occur in the surface ocean ?, *Geophys. Res. Lett.*, 37, 1–5, doi:10.1029/2010GL042574,
857 2010.
- 858 Sanders, R., Henson, S. A., Koski, M., La, C. L. De, Painter, S. C., Poulton, A. J., Riley, J., Salihoglu, B., Visser,
859 A., Yool, A., Bellerby, R. and Martin, A. P.: The Biological Carbon Pump in the North Atlantic, *Prog. Oceanogr.*,
860 129, 200–218, doi:10.1016/j.pocean.2014.05.005, 2014.
- 861 Savoye, N., Buesseler, K. O., Cardinal, D. and Dehairs, F.: ²³⁴Th deficit and excess in the Southern Ocean during
862 spring 2001: Particle export and remineralization, *Geophys. Res. Lett.*, 31(12), L12301–L12301,
863 doi:10.1029/2004GL019744, 2004.

864 Savoye, N., Benitez-Nelson, C., Burd, A. B., Cochran, J. K., Charette, M., Buesseler, K. O., Jackson, G. A., Roy-
865 Barman, M., Schmidt, S. and Elskens, M.: ^{234}Th sorption and export models in the water column: A review, *Mar.*
866 *Chem.*, 100, 234–249, doi:10.1016/j.marchem.2005.10.014, 2006.

867 Shelley, R. U., Roca-Martí, M., Castrillejo, M., Masqué, P., Landing, W. M., Planquette, H. and Sarthou, G.:
868 Quantification of trace element atmospheric deposition fluxes to the Atlantic Ocean ($>40^\circ\text{N}$; GEOVIDE,
869 GEOTRACES GA01) during spring 2014, *Deep Sea Res. Part I Oceanogr. Res. Pap.*, (June),
870 doi:10.1016/j.dsr.2016.11.010, 2016.

871 Stange, P., Bach, L. T., Le Moigne, F. A. C., Taucher, J., Boxhammer, T. and Riebesell, U.: Quantifying the time
872 lag between organic matter production and export in the surface ocean: Implications for estimates of export
873 efficiency, *Geophys. Res. Lett.*, 43, 1–9, doi:10.1002/2016GL070875, 2016.

874 Thomalla, S., Turnewitsch, R., Lucas, M. and Poulton, A.: Particulate organic carbon export from the North and
875 South Atlantic gyres: The $^{234}\text{Th}/^{238}\text{U}$ disequilibrium approach, *Deep Sea Res. Part II Top. Stud. Oceanogr.*, 53,
876 1629–1648, doi:10.1016/j.dsr2.2006.05.018, 2006.

877 Thomalla, S. J., Poulton, A. J., Sanders, R., Turnewitsch, R., Holligan, P. M. and Lucas, M. I.: Variable export
878 fluxes and efficiencies for calcite, opal, and organic carbon in the Atlantic Ocean: A ballast effect in action ?,
879 *Global Biogeochem. Cycles*, 22, 1–10, doi:10.1029/2007GB002982, 2008.

880 Tonnard, M., Donval, A., Lampert, L., Claustre, H., Ras, J., Dimier, C., Sarthou, G., Planquette, H., van der Merwe,
881 P., Boutorh, J., Cheize, M., Menzel, J.-L., Pereira Contraira, L., Shelley, R., Bowie, A. R., Tréguer, P., Gallinari,
882 M., Duprez de Gesincourt, F., Germain, Y. and Lherminier, P.: Phytoplankton assemblages along the GEOVIDE
883 section (GEOTRACES section GA01) using CHEMTAX, n.d.

884 Turner, A. and Millward, G. E.: Suspended Particles: Their Role in Estuarine Biogeochemical Cycles, *Estuar.*
885 *Coast. Shelf Sci.*, 55(6), 857–883, doi:10.1006/ecss.2002.1033, 2002.

886 Villa-Alfageme, M., Soto, F. C., Ceballos, E., Giering, S. L. C., Le Moigne, F. A. C., Henson, S., Mas, J. L. and
887 Sanders, R. J.: Geographical, seasonal and depth variation in sinking particle speeds in the North Atlantic,
888 *Geophys. Res. Lett.*, 43, 8609–8616, doi:10.1002/2016GL069233.Received, 2016.

889 Westberry, T., Behrenfeld, M. J., Siegel, D. A. and Boss, E.: Carbon-based primary productivity modeling with
890 vertically resolved photoacclimation, *Global Biogeochem. Cycles*, 22(2), 1–18, doi:10.1029/2007GB003078,
891 2008.

892 Zehr, J. P. and Ward, B. B.: Nitrogen Cycling in the Ocean : New Perspectives on Processes and Paradigms
893 MINIREVIEW Nitrogen Cycling in the Ocean : New Perspectives on Processes and Paradigms, *Appl. Environ.*
894 *Microbiol.*, 68(3), 1015–1024, doi:10.1128/AEM.68.3.1015, 2002.

895 Zúñiga, D., Villaceros-Robineau, N., Salgueiro, E., Alonso-Pérez, F., Rosón, G., Abrantes, F. and Castro, C. G.:
896 Particle fluxes in the NW Iberian coastal upwelling system: Hydrodynamical and biological control, *Cont. Shelf*
897 *Res.*, 123, 89–98, doi:10.1016/j.csr.2016.04.008, 2016.

898 Zunino, P., Lherminier, P., Mercier, H., Daniault, N., García-Ibáñez, M. I. and Pérez, F. F.: The GEOVIDE cruise
899 in May-June 2014 reveals an intense Meridional Overturning Circulation over a cold and fresh subpolar North
900 Atlantic, *Biogeosciences*, 14(23), 5323–5342, doi:10.5194/bg-14-5323-2017, 2017.

901

902

903

904

905

906

907

908
909
910
911
912
913
914
915
916
917
918
919

920 **Table 1:** Summary of the ^{234}Th export and scavenging fluxes using steady state (SS) and non-steady state (NSS) models. The
 921 ^{234}Th export fluxes using the SS model are calculated at the depths corresponding to the bottom of the primary production
 922 zone (PPZ), the equilibrium (Eq) depth and 100 m below Eq (Eq+100); the latter being used to estimate a remineralisation
 923 flux of ^{234}Th (R100). Negative R100 values indicate an increase of the export flux between Eq and Eq+100. Note that the
 924 depth was fixed to 100 m at Station 26 because of the lower sampling vertical resolution. Consequently, the export flux at
 925 Eq+100 and the R100 were not determined at Station 26.

Basin	Station		Export depth m	Th export (SS) dpm m ⁻² d ⁻¹	Th export (NSS) dpm m ⁻² d ⁻¹	Th scavenging (SS) dpm m ⁻² d ⁻¹	
Iberian	1	PPZ	155	1327 ± 137	1442 ± 80	1509 ± 189	
		Eq	90	1264 ± 104			
		Eq+100	190	1348 ± 199			
		R100		-84 ± 224			
	13	PPZ	82	1247 ± 99	1588 ± 86	2898 ± 285	
		Eq	110	1418 ± 111			
		Eq+100	210	1008 ± 187			
		R100		410 ± 218			
West European	21	PPZ	82	1723 ± 82	2352 ± 70	3917 ± 212	
		Eq	110	1873 ± 97			
		Eq+100	210	1513 ± 235			
		R100		360 ± 255			
	26	PPZ	95	1432 ± 117	1968 ± 98	2839 ± 220	
		Fixed	100	1486 ± 117			
	Icelandic	32	PPZ	75	1455 ± 92	3540 ± 113	3690 ± 199
			Eq	130	2282 ± 119		
Eq+100			230	2200 ± 227			
R100				81 ± 256			
38		PPZ	70	1136 ± 80	2345 ± 115	1495 ± 160	
		Eq	80	1134 ± 95			
		Eq+100	180	949 ± 151			
		R100		185 ± 178			
Irminger	44	PPZ	37	321 ± 66	516 ± 90	1802 ± 71	
		Eq	40	321 ± 66			
		Eq+100	140	454 ± 114			
		R100		-132 ± 132			
	51	PPZ	37	495 ± 67	1625 ± 108	2189 ± 260	
		Eq	100	922 ± 103			
		Eq+100	200	873 ± 114			
		R100		49 ± 154			
Labrador	64	PPZ	83	853 ± 129	1423 ± 122	1142 ± 192	
		Eq	80	855 ± 95			
		Eq+100	180	733 ± 200			
		R100		123 ± 221			
	69	PPZ	35	684 ± 57	1068 ± 53	1257 ± 112	
		Eq	40	758 ± 57			
		Eq+100	140	357 ± 148			
		R100		401 ± 159			
77	PPZ	55	693 ± 77	1169 ± 75	1529 ± 148		
	Eq	60	696 ± 77				
	Eq+100	160	444 ± 146				
	R100		252 ± 165				

926 **Table 2:** Comparison of the steady state POC export fluxes at Eq as determined using the POC:²³⁴Th ratios in the large
927 (LSF; > 53 μm) and small size fraction (SSF; 1-53 μm).

928

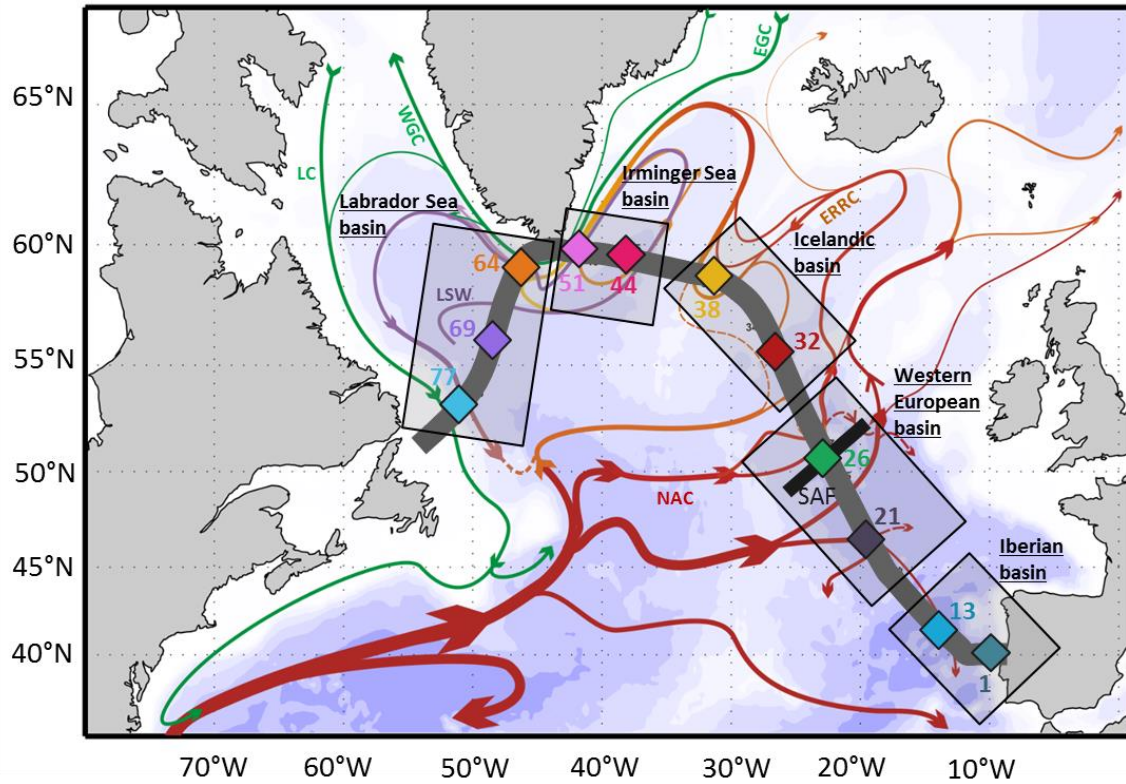
929

Basin	Station #	LSF POC flux mmol m ⁻² d ⁻¹	SSF POC flux mmol m ⁻² d ⁻¹
Iberian	1	12 ± 22	6.9 ± 2
	13	2.2 ± 0.3	3.3 ± 0.6
west European	21	4.8 ± 0.8	6.3 ± 1.4
	26	7.9 ± 5.0	6.1 ± 3.7
Icelandic	32	8.3 ± 0.5	8.8 ± 0.5
	38	4.8 ± 0.4	5.2 ± 0.7
Irminger	44	1.4 ± 0.5	2.4 ± 0.5
	51	2.7 ± 0.3	3.8 ± 0.5
Labrador	64	7.8 ± 1.5	5.5 ± 4.9
	69	10 ± 1	13 ± 1
	77	6.1 ± 1.5	7.5 ± 0.9

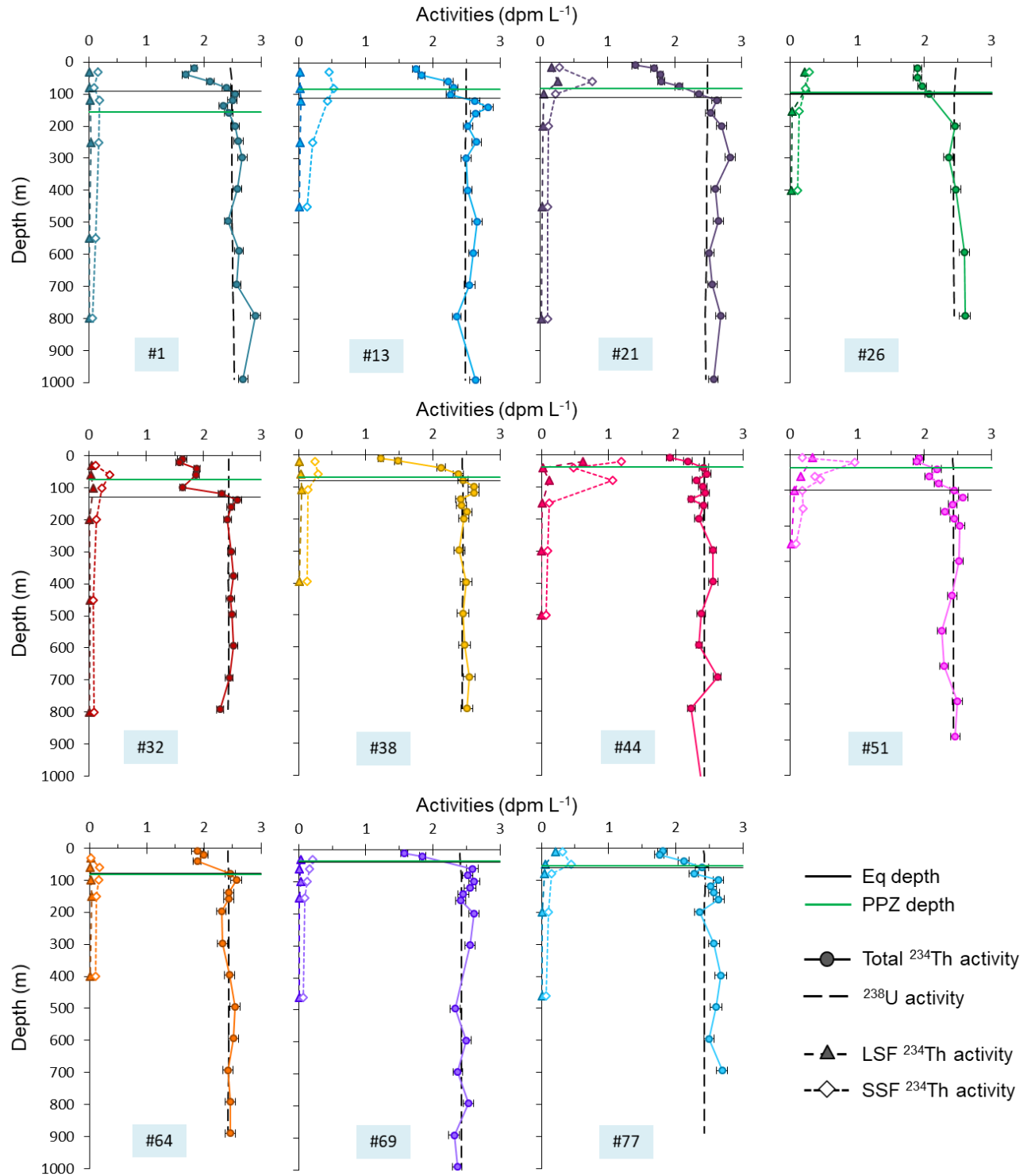
930

931 **Table 3:** POC (particulate organic carbon) to ^{234}Th ratios (in $\mu\text{mol dpm}^{-1}$) in the LSF, POC export fluxes (in $\text{mmol m}^{-2} \text{d}^{-1}$), *in-situ* primary production (PP; Fonseca-Batista
 932 et al., 2018 and this study) and satellite-derived PP from the Vertically Generalized Production Model (VGPM-PP) integrated over 8 days, 32 days and over the whole
 933 season (in $\text{mmol m}^{-2} \text{d}^{-1}$) and the POC fluxes at Eq+100 m (in $\text{mmol m}^{-2} \text{d}^{-1}$). Because of the lower vertical sampling resolution at Station 26, no POC export flux was
 934 determined at Eq+100. *The sampling to determine the *in-situ* PP at Station 51 occurred 24 h after the sampling of the particulate ^{234}Th and POC.

Station	POC: ^{234}Th at Eq	POC flux at Eq	<i>in-situ</i> PP	8-days VGPM-PP	32-days VGPM-PP	seasonal VGPM-PP	POC flux at Eq+100
#	$\mu\text{mol dpm}^{-1}$	$\text{mmol m}^{-2} \text{d}^{-1}$	$\text{mmol m}^{-2} \text{d}^{-1}$	$\text{mmol m}^{-2} \text{d}^{-1}$	$\text{mmol m}^{-2} \text{d}^{-1}$	$\text{mmol m}^{-2} \text{d}^{-1}$	$\text{mmol m}^{-2} \text{d}^{-1}$
1	9 ± 17	12 ± 22	33 ± 2	76 ± 3	80 ± 11	96 ± 62	5.3 ± 23.2
13	1.6 ± 0.2	2.2 ± 0.3	79 ± 3	64 ± 7	72 ± 18	81 ± 63	0.7 ± 0.2
21	2.6 ± 0.4	4.8 ± 0.8	135 ± 2	161 ± 21	260 ± 97	201 ± 119	2.3 ± 0.4
26	5.3 ± 3.3	7.9 ± 5.0	174 ± 19	77 ± 14	74 ± 19	112 ± 59	
32	3.6 ± 0.1	8.3 ± 0.5	105 ± 11	105 ± 7	95 ± 13	87 ± 13	6.5 ± 0.7
38	4.2 ± 0.1	4.8 ± 0.4	68 ± 7	82 ± 5	94 ± 34	109 ± 32	3.5 ± 0.6
44	4.4 ± 1.3	1.4 ± 0.5	137 ± 2	89 ± 3	110 ± 65	101 ± 66	0.8 ± 0.4
51	2.9 ± 0.01	2.7 ± 0.3	*166 ± 32	95 ± 7	125 ± 118	125 ± 118	1.7 ± 0.2
64	9.2 ± 1.1	7.8 ± 1.5	54 ± 18	59 ± 18	109 ± 115	103 ± 122	4.9 ± 1.5
69	14 ± 0.04	10 ± 1	27 ± 5	108 ± 8	134 ± 80	134 ± 80	3.1 ± 1.3
77	8.8 ± 1.9	6.1 ± 1.5	80 ± 21	108 ± 8	134 ± 80	134 ± 80	3.1 ± 1.3

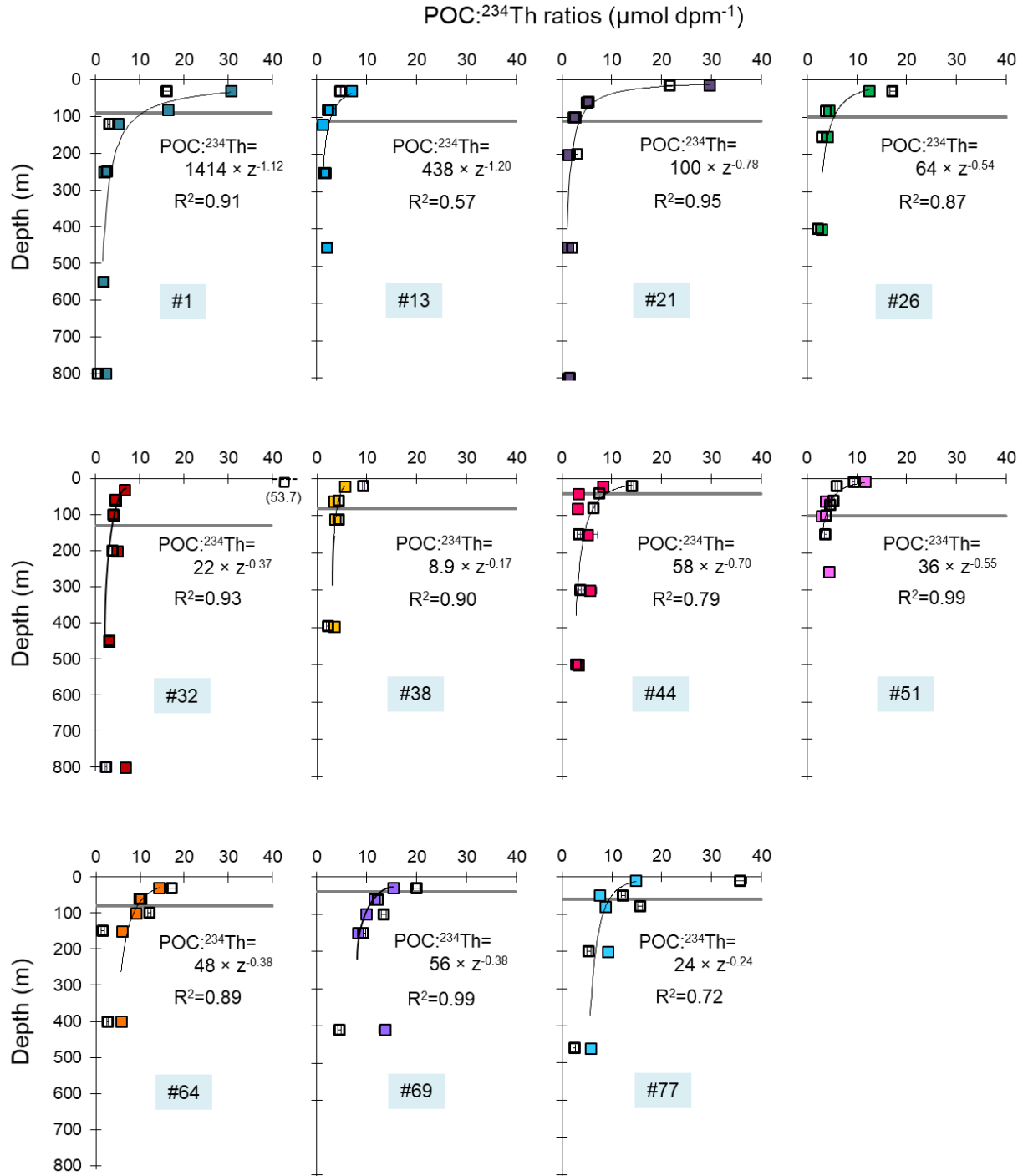


936
 937 **Figure 1:** Simplified schematic of the surface circulation in the North Atlantic (adapted from Danialt et al., 2016)
 938 superimposed with the GEOVIDE cruise track (thick grey line) and stations (colored diamonds). Main surface currents are
 939 indicated: East Greenland Current (EGC), West Greenland Current (WGC), Labrador Current (LC), Eastern Reykjanes
 940 Ridge Current (ERRC), North Atlantic Current (NAC). The Sub-Arctic Front (SAF) and the Labrador Seawater (LSW)
 941 when in surface (i.e. within the Labrador basin) are also represented. The color codes for sampled stations are also used in
 942 the following figures.



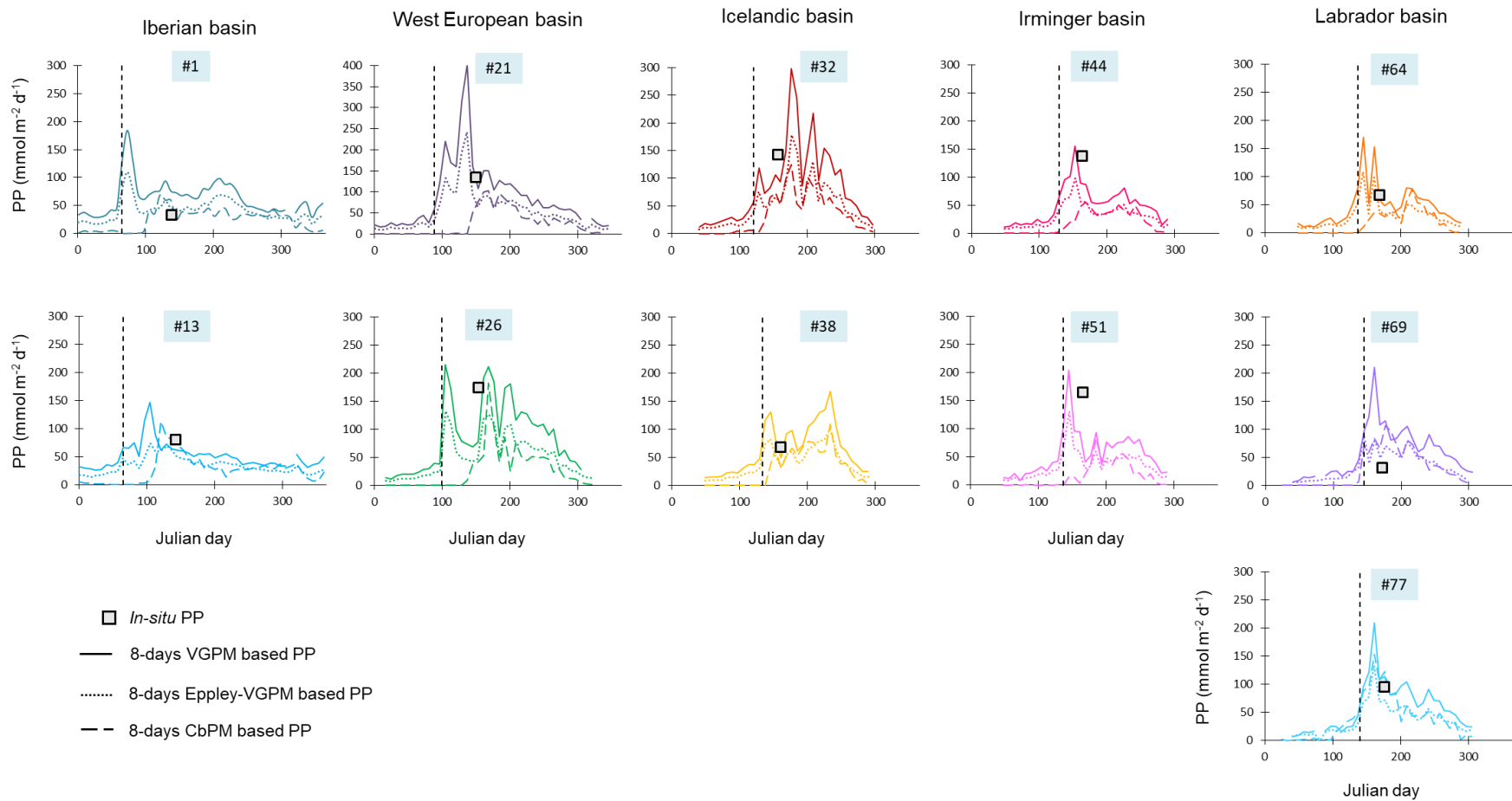
943

944 **Figure 2:** Profiles of the total ^{234}Th (closed circles), total ^{238}U (black dotted vertical line) and particulate ^{234}Th activities for
 945 the small size fraction (SSF; 1-53 μm ; open diamonds) and for the large size fraction (LSF; $>53\ \mu\text{m}$; closed triangles). All
 946 activities are expressed in dpm L^{-1} . The horizontal black line is the Eq depth (depth where ^{234}Th returns to equilibrium with
 947 ^{238}U), and the horizontal green line is the depth of the PPZ (primary production zone). Error bars are plotted but may be
 948 smaller than the size of the symbols. Note that the Eq depth at Station 26 is fixed at 100 m because of the lower sampling
 949 vertical resolution.



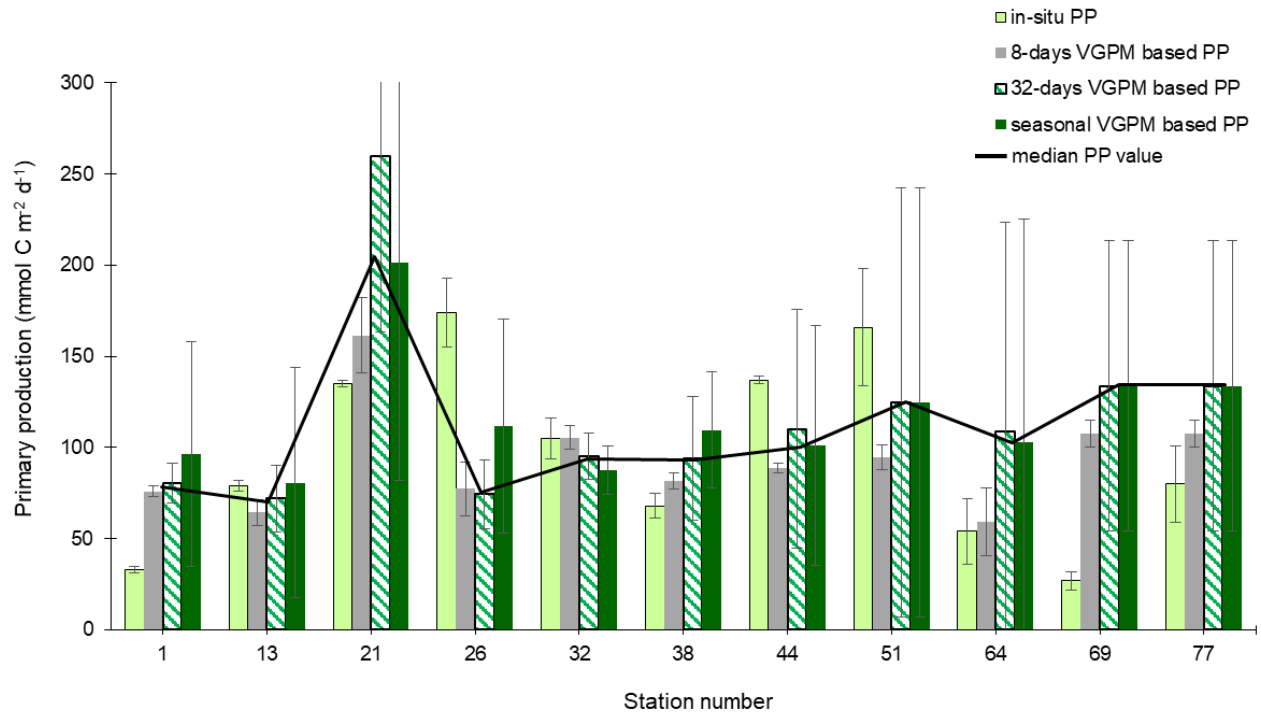
950

951 **Figure 3:** Profiles of the POC:²³⁴Th ratios (μmol dpm⁻¹) in the SSF (open symbols) and LSF (closed symbols). The Eq depth,
 952 where ²³⁴Th is back to equilibrium with ²³⁸U, is indicated with the grey horizontal line. The thin black line represents the
 953 power law fit ($POC:^{234}Th = a \times Z^{-b}$) of the LSF. The median percentage errors on POC:²³⁴Th ratios are respectively
 954 representing 5 and 6% of the value for the SSF and the LSF. Error bars are plotted but may be smaller than the size of the
 955 symbols.



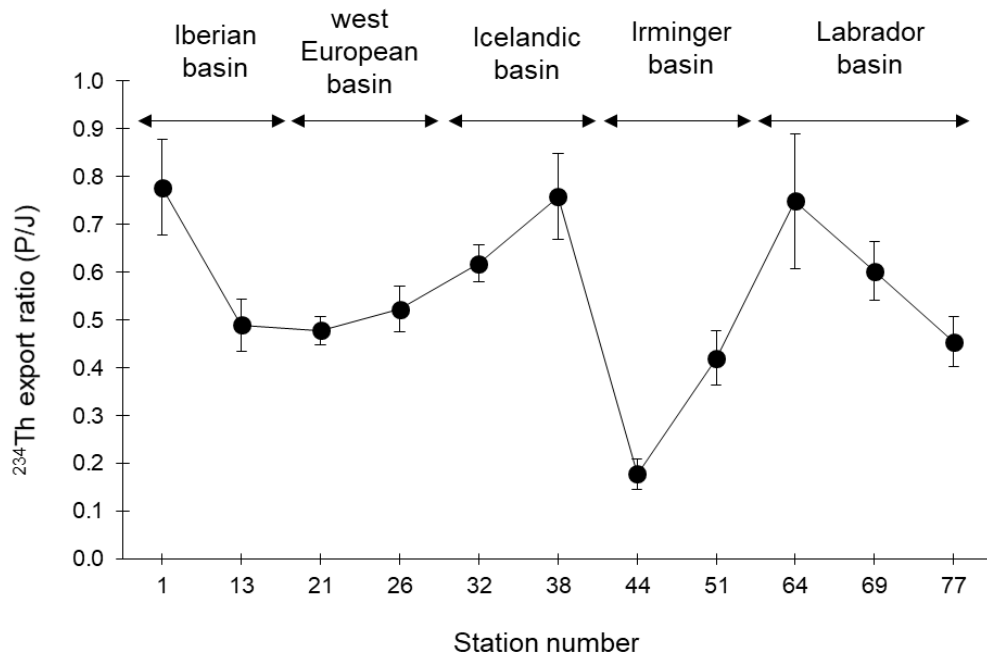
956

957 **Figure 4:** *In-situ* (squares) and satellite VGPM-derived (continuous lines), VGPM-Eppley-derived (dotted lines) and CbPM-derived (dashed lines) primary production (PP;
 958 in $\text{mmol m}^{-2} \text{d}^{-1}$) data at the time of our sampling and along the year 2014. The start of the bloom, defined by a PP increase of 30% above the winter value, is indicated
 959 with the black vertical dashed line.



960
961
962

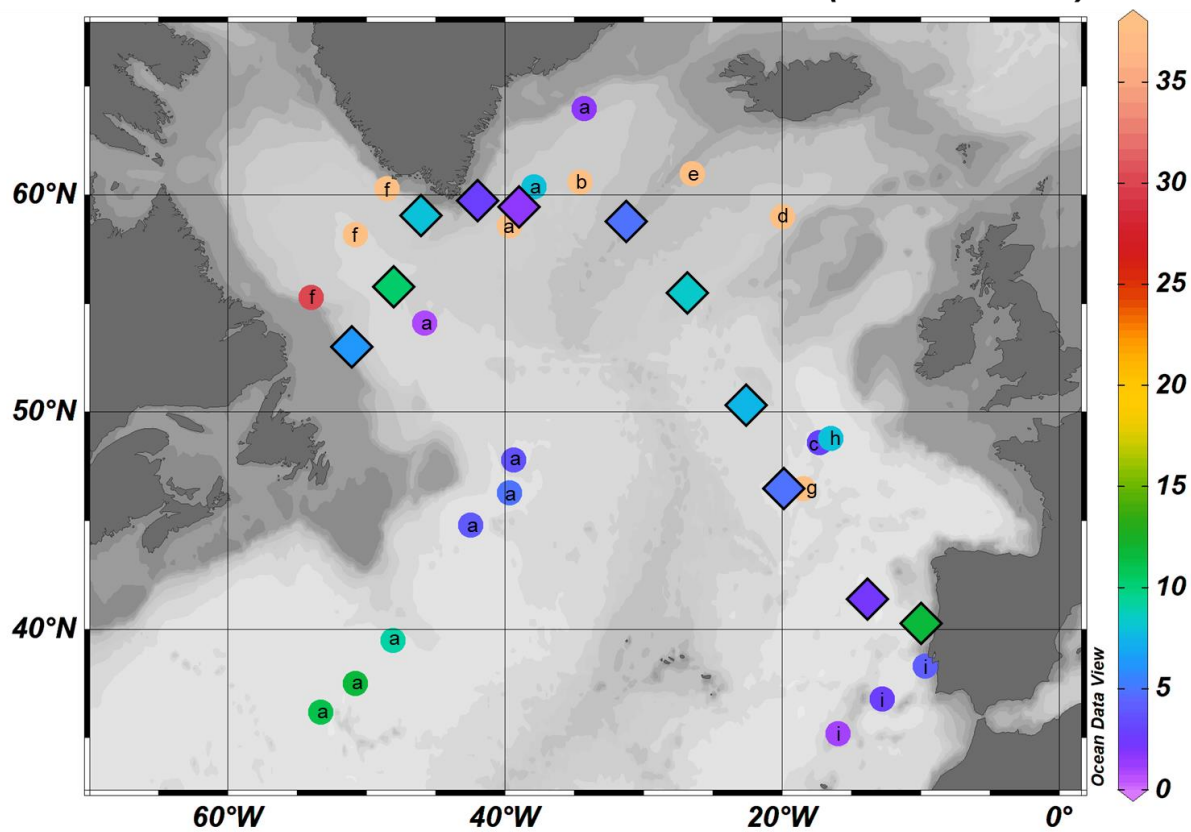
Figure 5: Comparison of *in-situ* and satellite VGPM (8-days, 32-days and seasonal averages) primary productivities ($\text{mmol m}^{-2} \text{d}^{-1}$) along the GEOVIDE transect. The median of the four values is also indicated (black line).



963

964 **Figure 6:** Variability of the ^{234}Th export ratio (i.e., the ratio of the ^{234}Th export flux over the ^{234}Th scavenged flux; P/J ratio)
 965 along the GEOVIDE section.

POC flux ($\text{mmol m}^{-2} \text{d}^{-1}$)



966

967 **Figure 7:** Comparison of the POC export fluxes from this study (diamonds with black borders) with other ^{234}Th -derived
 968 estimates of POC exports in the North Atlantic (a: Puigcorb  et al., 2017; b: Ceballos-Romero et al., 2016; c: Thomalla et
 969 al., 2008; d: Sanders et al., 2016; e: Martin et al., 2011; f: Moran et al., 2003; g: Buesseler et al., 1992; h: Le Moigne et al.,
 970 2013; i: Owens et al., 2015).

971

972

973

974

975

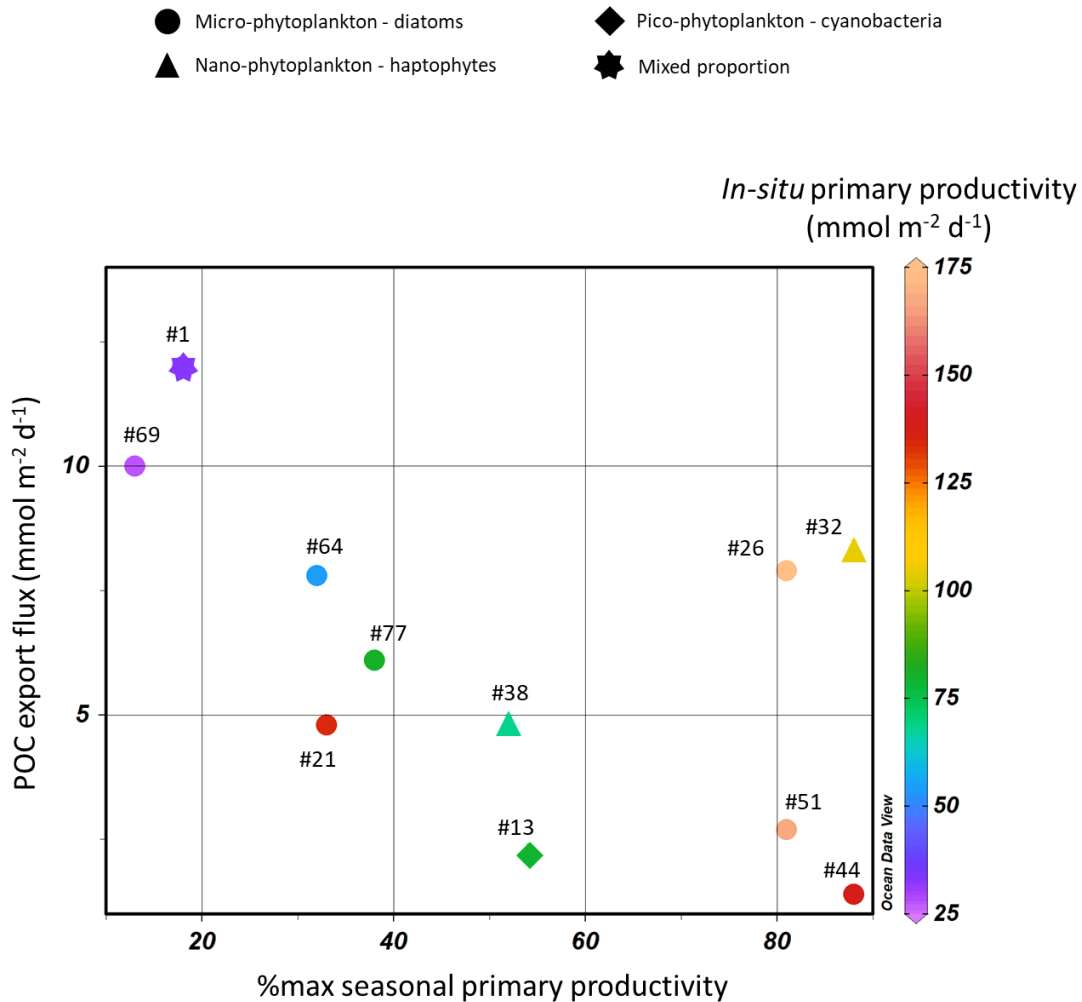
976

977

978

979

980



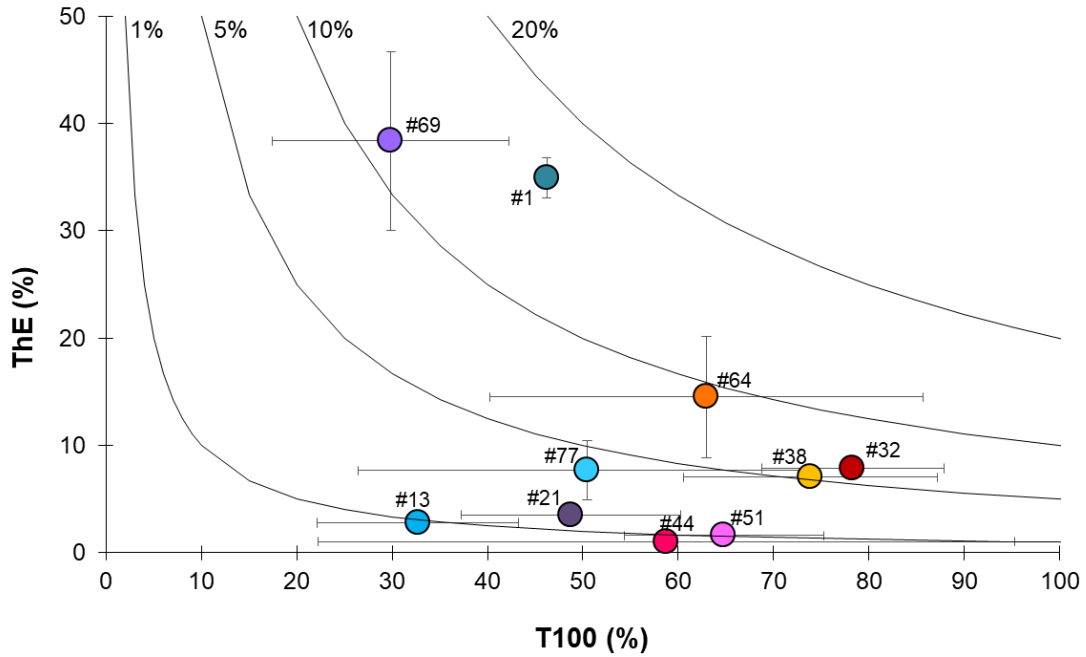
981

982 **Figure 8: Percentage of the *in-situ* primary productivity (PP) relative to the maximal V_{CDM}-PP along the season (%max**
 983 **seasonal primary productivity) in function of the POC export fluxes determined at the Eq depth. The %max**
 984 **seasonal primary productivity illustrates the stage of the bloom (i.e., a %max seasonal primary productivity**
 985 **equalling 100% corresponds to a sampling time at the bloom peak). This relationship is significant when not taking**
 986 **into account the stations sampled between two PP peaks (Stations 26, 32 and 38, see Fig. 4): R²=0.77 and p-**
 987 **value<0.01. The *in-situ* PP measured at sampling time is indicated with the colours in order to indicate the bloom**
 988 **intensity. The dominating phytoplankton community is also indicated, with circles indicating micro-phytoplankton**
 989 **dominance (with a majority of diatoms), triangles nano-phytoplankton dominance (with a majority of haptophytes)**
 990 **and diamonds pico-phytoplankton dominance (with a majority of cyanobacteria). Note that Station 1 is represented**
 991 **by a star because of the mixed proportion of micro-, nano- and pico-phytoplankton.**

992

993

994



995

996 **Figure 9:** Export efficiency (ThE = Export at Eq / *in-situ* PP) versus transfer efficiency (T100 = Export flux at Eq+100 /
 997 Export flux at Eq). The black lines represent the modelled 1, 5, 10 and 20% of PP exported to depths > Eq+100 m.